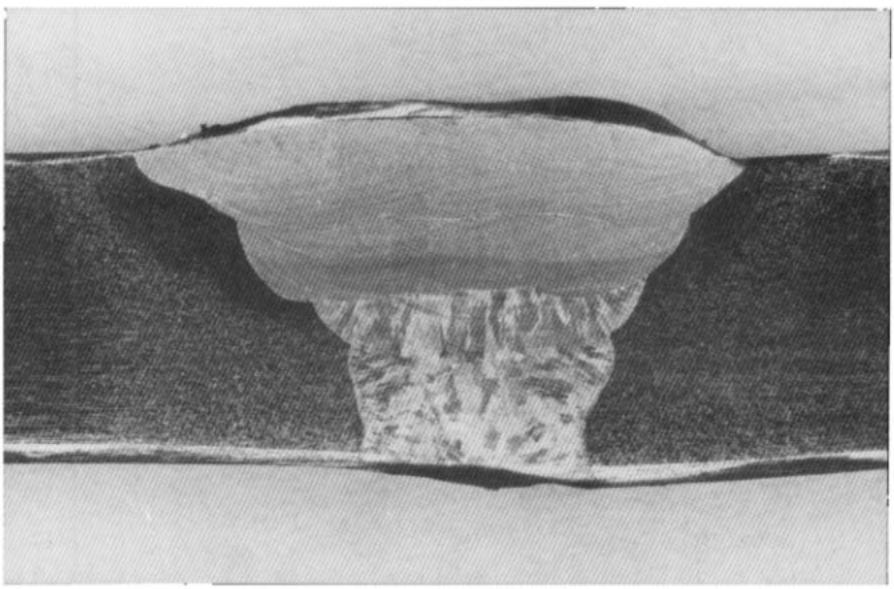
NORD

SEPTEMBER 1989

INTERGRANULAR STRESS CORROSION CRACKING



nka

Nordic
liaison committee for
atomic energy

nka

Nordisk kontaktorgan for atomenergispørgsmål | Nordiska kontaktorganet för atomenergifrågor | Pohjoismainen atomienergia-yhdyselin | Nordic liaison committee for atomic energy

INTERGRANULAR STRESS CORROSION CRACKING

Final Report of the NKA-Project MAT 530

Edited by:
Hannu Hänninen
VTT, Finland

September 1989

The present report is available from:

Technical Research Centre of Finland (VTT)
Metals Laboratory, Library
Box 26
SF-02151 ESBO, Finland

The front cover shows a stainless steel welding that has been etched to disclose the weld structure and to reveal areas that are susceptible to intergranular stress corrosion cracking.

ISBN 87-7303-347-2

NORD 1989:74

Graphic Systems AB, Malmö 1989

ABSTRACT

An austenitic stainless steel pipe weldment, which had been in operation in the Ringhals 1 reactor was characterized by using an electrochemical sensitization testing method (EPR) as well as with transmission electron microscopy. Specimens were cut from the studied pipe far from the weld and heat treated. A Nordic EPR "round robin" test was performed to measure the degree of sensitization of the material.

Critical stress corrosion potential for the heat affected zone was determined in high temperature pure water by using slow strain rate testing.

Key words: Stress corrosion cracking, austenitic stainless steel, BWR, sensitization, transmission electron microscopy, EPR-method, slow strain rate testing

This report is a part of the safety programme sponsored by NKA, the Nordic Liaison Committee for Atomic Energy, 1985-1989. The project work has partly been financed by the Nordic Council of Ministers.

SUMMARY

Stress corrosion cracking of piping materials may have serious consequences on safety as well as on the economy of a nuclear plant. For stress corrosion cracking to occur in a weldment three conditions must be simultaneously present: (1) a susceptible material, (2) a tensile stress, and (3) a chemical environment that will facilitate cracking. If austenitic stainless steels such as AISI 304 are subjected to temperatures in the range of 500 - 800 °C as a result of heat treatment or welding, chromium-rich carbides may precipitate on grain boundaries and cause localized chromium depletion. This produces sensitization, i.e., an increased susceptibility to intergranular corrosion and intergranular stress corrosion cracking. The latter has been observed in several boiling water reactor systems.

There are a number of standardized tests to assess the susceptibility for intergranular corrosion, but none fulfill the demands of being both quantifiable and non-destructive. They are therefore not suitable for field testing on systems in service. For this purpose a new technique is promising, the electrochemical potentiokinetic reactivation (EPR) technique. It involves analysis of electrochemical polarization curves taken up in a sulphuric acid/thiocyanate solution. One of the objectives of this study is to assess the EPR-technique by using it to evaluate the degree of sensitization in AISI 304 stainless steel pipes, both furnace sensitized and welded. In both cases similar tests were performed at various Nordic and Italian laboratories and the results were compared.

EPR measurements were performed (using both the single loop, SL, and double loop, DL, variants of the method) on specimens which had been furnace sensitized for various times at 620 °C. The two methods showed comparable reproducibility and correlated well with each other. Small variations in the surface preparation techniques (polishing or polishing + etching for SL, grinding to 600 or 120 grit for DL) did not have any systematic effect on the EPR results. Major variations in EPR-results are caused by test temperature and grain size.

In the case of the welded specimen, which had been in service in the Ringhals-1 reactor for 45 000 hours at 230 °C, EPR measurements were made for the heat affected zone close to the weld. The inner and outer pipe surfaces were investigated first. Then the specimen was cut parallel to the fusion line into sections, 1 - 2 mm thick, and EPR measure-

ments were performed on the sections to determine the variation in the degree of sensitization with distance from the weld. A maximum level of sensitization was found at 2-3 mm from the fusion line using both the single and double loop variants of the EPR. Oxalic acid testing (according to ASTM A262 Practice A) to assess susceptibility to intergranular corrosion was also performed on longitudinal sections of the weld and the resulting etch structures evaluated using "IBAS" image analysis. This showed qualitatively similar results with a maximum degree of sensitization 3-4 mm from the fusion line. Both EPR and oxalic acid etching results were also correlated to transmission electron microscopy studies of carbide precipitation and chromium depletion in the heat affected zone.

Intergranular stress corrosion testing of the welded specimens with two polarization techniques revealed the critical potential for cracking to be about -100 mV(SHE) and that cracking took place at distance of 3 - 5 mm from the fusion line.

The EPR measurements performed on the inner and outer pipe surface suggest that care should be exercised in applying published acceptance limits for EPR measurements on welded materials. The external (practically accessible) surface in this investigation showed an acceptably low level of sensitization. However, the inner surface (which is exposed to the corrosive environment) was heavily sensitized as a result of the repeated heating associated with successive welding passes. The possible role of low temperature sensitization could not be verified.

Not only nuclear industry but also e.g. chemical industry and thermal power plants have corrosion problems of this kind. If non-destructive measurement of the degree of sensitization and knowledge of threshold corrosion potential for cracking to occur would become available, then the maintenance expences and outage costs could be reduced.

SAMMANFATTNING

Spänningskorrosion av konstruktionsmaterial i reaktorers rörledningar kan förorsaka allvarliga konsekvenser, både säkerhetsmässigt och i ekonomiskt avseende. För att spänningskorrosion skall uppträda måste tre villkor samtidigt vara uppfyllda: (1) korrosionsbenäget material, (2) dragspänning, och (3) en kemisk miljö, som främjer sprickning. Om austenitiska rostfria stål som t.ex. SS2333 utsätts för temperaturer inom området 500 - 800 °C på grund av värmebehandling eller svetsning kan kromkarbider utskiljas vid korngränser och orsaka kromutarmning i den närliggande grundmassan. Detta resulterar i sensibilisering eller en ökad benägenhet till både interkristallin korrosion och interkristallin spänningskorrosion. Det senare har visat sig vara ett allvarligt problem i kokarreaktorsystem.

Det finns ett antal standardiserade metoder för att utvärdera benägenheten till interkristallin korrosion. Ingen av dessa erbjuder emellertid möjlighet till både oförstörande fältprovning på befintliga system och att ge kvantitativa mått på graden av sensibilisering. Den elektrokemiska potentiokinetiska reaktivationstekniken (EPR), som innebär analys av polarisationskurvor upptagna i svavelsyra/tiocyanatlösning, uppfyller däremot båda de ovannämnda kraven. Målet med detta arbete var att utvärdera EPR-tekniken genom tillämpning på såväl ugnssensibiliserat som svetssensibiliserat SS2333 rostfritt material med kolhalten 0.052 %. Samma typ av mätningar genomfördes parallellt vid ett antal laboratorier och resultaten jämfördes.

EPR-mätningar genomfördes enligt två metoder (single loop, SL, och double loop, DL) på prover vilka ugnssensibiliserats olika tider vid 620 °C. De två metoderna visade god korrelation och jämförbar reproducerbarhet. Små variationer i provberedningstekniken (polering eller polering + etsning för SL, slipning till 600 eller 120 ytfinhet för DL) hade ingen systematisk inverkan på EPR-resultaten. Variationer i testtemperatur och mätning av materialets kornstorlek orsakade de största variationerna i resultatet.

Det svetsade provet hade varit i drift i Ringhals-1 reaktorn vid 230 °C under 45 000 timmar. I detta fall gjordes EPR-mätningar först på de yttre och inre rörytorna i den värmepåverkade zonen intill svetsen. Provet kapades sedan i 1 - 2 mm tjocka skivor parallellt med svetsgränsen och EPR-mätningar gjordes på dessa för att bestämma sensibiliseringsgraden som funktion av avståndet från svetsen. Den högsta sensibiliseringen uppmättes 2 - 3 mm från smältgränsen med både SL och DL teknikerna. Överensstämmelsen var god mellan EPR-mätningarna och oxalsyraprovning (enligt ASTM A262 Practice A) vilka genomförts i avsikt att bestämma benägenheten till interkristallin korrosion. Oxalsyra-

provning gjordes på ett längsgående tvärsnitt på den värmepåverkade zonen, resulterande etsstrukturer analyserades med "IBAS" bildanalyssystemet och visade ett sensibiliseringsmaximum 3 - 4 mm från smältgränsen. Resultaten från både EPR och oxalsyraprovning har även korrelerats till ATEM (analyserande transmissionselektronmikroskop) och TEM studie av karbidutskiljningar och kromutarmning i materialet.

Interkristallin spänningskorrosionsprovning utfördes på samma svetsar med två olika metoder för att kontrollera korrosionspotential. Tröskelpotential för interkristallin spänningskorrosion var ungefär -100 mV(SHE) för detta material. Sprickorna initierade i området 3 - 5 mm från smältlinjen.

EPR-mätningarna som gjordes på de inre och yttre rörytorna visar att publicerade gränsvärden för EPR-mätningar på svetsat material måste tillämpas med försiktighet. I den undersökta svetsen visade den yttre (praktiskt tillgängliga) rörytan en acceptabelt låg sensibiliseringsgrad. Den inre ytan (som exponerades mot den korrosiva miljön) var emellertid kraftigt sensibiliserad p.g.a. värmepåverkan från flera svetssträngar lagda i ett senare stadium av svetsningsoperationen. Möjlig lågtemperatur sensibilisering i materialet kunde inte bestämmas kvantitativt, eftersom samma material inte fanns som referens.

Förutom kärnkraftsindustrin har även kemisk industri och värmekraftverk korrosionsproblem av detta slag. Om oförstörande mätning av sensibiliseringsgraden och kunskap om kritisk potential för sprickning vore mera tillgängliga, kunde underhållskostnaderna och dyra driftavbrott reduceras.

C O N T E N T S

		Page
1.	INTRODUCTION	1
2.	SENSITIZATION OF AUSTENITIC STAINLESS STEELS	2
3.	EPR-ROUND ROBIN	4
3.1	IM, Sweden	5
3.2	Studsvik, Sweden	6
3.3	VTT, Finland	6
3.4	ENEA, Italy	6
3.5	CISE, Italy	7
3.6	Temperature dependence of EPR measurements (IM, Sweden)	7
3.7	EPR-round robin results	7
3.8	Conclusions	11
4.	MATERIAL CHARACTERIZATION	13
4.1	Measurement of the DOS	13
4.2	Electron microscopy	16
4.3	Correlation of DOS to TEM/ATEM investigations	18
4.4	Conclusions	18
5.	STRESS CORROSION TESTING	21
5.1	Slow strain rate tests	21
5.2	Multipotential tests with U-bend specimens	22
5.3	Test results	22
5.4	Conclusions	23
6.	GENERAL CONCLUSIONS	25
7.	REFERENCES	27
	Tables	31
	Figures	40

1. INTRODUCTION

In the present final report the most important results of the NKA project MAT 530 INTERGRANULAR STRESS CORROSION CRACKING are summarized. Those readers who are interested in more details are directed to apply to subreports and other publications issued earlier (1 - 11).

The main object of the project was to study the possible ageing of the austenitic stainless steel weld heat affected zones during reactor operation and resulting low temperature sensitization (LTS). LTS causes increased susceptibility to Intergranular Stress Corrosion Cracking (IGSCC) in the Boiling Water Reactor (BWR) conditions. The studied pipe material was removed from Ringhals 1 BWR-plant from hydraulic scram system after about 45 000 hours of operation at 230 °C after detection of extensive IGSCC in the system.

The second theme of the project was to perform a Nordic round robin on Electrochemical Potentiokinetic Reactivation (EPR) testing method, which can be suitably used for non-destructive detection of sensitization and measurement of the degree of sensitization (DOS) of the stainless steels even directly from the component in the field. Also the threshold electrochemical potential for IGSCC was measured by using two different test techniques.

The project was financed, besides by NKA, partly also by the Swedish Nuclear Power Inspectorate (SKI) and by the Ministry of Trade and Industry of Finland. The companies and research institutes, which have participated, and their representatives are listed on page 3 of the cover.

2. SENSITIZATION OF AUSTENITIC STAINLESS STEELS

Intergranular stress corrosion cracking (IGSCC) of austenitic stainless steels, usually AISI 304 steel, is a serious problem in boiling water reactors (BWR). It is associated with the simultaneous presence of a number of factors: stress (service stress, thermal stress or residual stress), a critical environment (high purity water containing oxygen) and sensitization. Sensitization in Type 304 stainless steels occurs when they are subject to temperatures in the range ~ 500 - 800 °C, either as a result of heat treatment or welding, so that chromium-rich carbides ($M_{23}C_6$) precipitate at grain boundaries, deplete the adjacent matrix of chromium and, thus, render the material susceptible to intergranular corrosive attack. The fact that, in the vast majority of cases, IGSCC has occurred in the heat affected zone (HAZ) adjacent to welds underlines the importance of sensitization as a contributory factor and emphasises the need for understanding and quantification of the sensitization process.

There are a number of methods of measuring the degree of sensitization (DOS) which have been standardized by ASTM and others. Four of these methods, ASTM A262 Practices B to E otherwise known as the Streicher, Huey, Warren and Strauss tests, respectively, involve prolonged exposure of the steel to boiling acid solutions and are as such destructive methods inapplicable to field testing. ASTM Practice A involves electrolytic etching in oxalic acid followed by a metallographical assessment of the etch structure and is thus non-destructive and suitable for field use. However, in its present form this method gives only a qualitative and not a quantitative measure of the DOS. The EPR (Electrochemical Potentiokinetic Reactivation) method is an electrochemical method for assessing sensitization originally proposed by Cihal et al. (12). The method is not yet standardized but is under the jurisdiction of ASTM Committee G-1 on Corrosion of Metals (13). The EPR test method satisfies both demands of quantifiability and applicability to field testing. A number of comparative studies have shown good agreement between EPR-measurements and other intergranular corrosion tests (14-20) and even a good correlation to dynamic slow strain rate testing (SSRT) of intergranular stress corrosion cracking susceptibility (15). Best agreement is observed between EPR measurements and Strauss testing as both attack the chromium depleted zones at grain boundaries. This is illustrated by Fig. 1, which shows the polarization curves for an AISI 304 (18Cr10Ni) alloy and a simulated grain boundary alloy (10Cr10Ni). The corrosion potential in the Strauss test is similar to the applied potential in the EPR test and reveals sensitization by the difference in active dissolution rate of Cr-depleted grain boundaries and unsensitized material. Oxalic acid etching involves much higher potentials and primarily attacks the chromium-rich $M_{23}C_6$ carbides

rather than the chromium depleted zones (18). It may thus under some circumstances be expected to give somewhat different results.

The main objective of this project is to evaluate the EPR technique by using it to determine the degree of sensitization (DOS) in an AISI 304 stainless steel pipe weldment. Specimens were of two types: firstly, furnace-sensitized material being used in a European round robin on EPR measurements and, secondly, welded specimens. The latter had suffered sensitization in the heat affected zone as a result of welding and had also been in service in Ringhals 1 BWR-plant for about 45 000 hours at a temperature of 230 °C. This could have resulted in low temperature sensitization (LTS), i.e., a further growth of carbides nucleated during welding and increased Cr-depletion adjacent to grain boundaries. In the case of the welded specimens results are compared with those from Strauss test and oxalic acid etching and correlated to ATEM and TEM investigations of carbide precipitation and chromium depletion, EPR measurements and intergranular stress corrosion cracking tests on the same material.

3. EPR-ROUND ROBIN

The electrochemical potentiokinetic reactivation (EPR) technique is an electrochemical method for assessing sensitization which satisfies both demands of quantifiability and applicability to field testing. Clarke et al. (15, 20) proposed a standard testing method (13). There are two variants of the technique, denoted the single loop (SL) and double loop (DL) methods, but both have the common feature of involving evaluation of a polarization curve for the materials in question in a sulfuric acid/potassium thiocyanate solution. In the single loop case (Fig. 2) the dissolution charge Q is measured and normalized to the grain boundary area (obtained from the ASTM grain size) to yield the P_a value which is a measure of the degree of sensitization.

$$P_a(Ccm^{-2}) = \frac{Q}{GBA} \qquad (1)$$

$$GBA = A_s\ [5.09544 \times 10^{-3} \exp(0.34696X)] \qquad (2)$$

where A_s = specimen area (cm^2)

X = ASTM grain size measured at 100x magnification.

In the double loop case it is the ratio I_r/I_a between the peak currents on the reverse and anodic scans which is employed, thus eliminating the need for metallographic evaluation of the grain size. Alternatively a P_a value may be evaluated from integration of the reverse potentiodynamic scan. Microscopic examination of the specimen after the reactivation procedure is always necessary in case of single loop method to confirm the morphology of the corrosion attack.

The present work reports the results of a Nordic round robin to evaluate the EPR testing method. In addition to the three participating Nordic laboratories (Swedish Institute for Metals Research (IM), Technical Research Centre of Finland (VTT) and Studsvik Energiteknik (SE)), EPR-testing was also performed at ENEA, Division Chemica, Italy (principal investigator A. Mignone) and CISE, Italy (principal investigator F. Uberti). Both the single loop and double loop EPR methods were employed but in both cases evaluation was based on the integrated current. The material investigated was the Ringhals 1 pipe steel, AISI 304 stainless steel (Table 1) with 0.052 % C, which was sensitized for various times at 620 °C to produce a wide variation in the degree of sensitization. Also reported are the results of single loop measurements to investigate the effect of testing temperature on P_a values (6).

For the round robin, specimens were heat treated at the Technical Research Centre of Finland (VTT) for 1, 10 and 24 hours at 620 °C then water quenched. For analysis of the temperature dependence of EPR measurements heat treatment was performed at the Swedish Institute for Metals Research (IM), and times of 0.5, 1, 3, 6, 9.5, 16 and 24 hours at the same temperature were employed.

3.1 IM, Sweden

An electrochemical cell of volume 3 liters was employed and the same solution used for three or four measurements. A platinum counter electrode was employed and a calomel reference electrode separated from the test solution by a salt bridge. The solution was deaerated both before and during the test with argon and the temperature maintained at 30 °C ± 1 °C by means of an immersion heater controlled by the potentiostat (Santron EMS). The external pipe surface of each specimen was ground flat and a copper wire spot welded to the reverse side. The whole assembly was then mounted in cold setting plastic to expose only the external pipe surface. This was ground and/or polished then masked down to a circle of area 1 cm^2 using Lacomit lacquer.

For the single loop method surface preparation of polishing to 1 μm as recommended by Clarke et al. (15) was employed, alternatively polishing followed by etching for 50 seconds in 2 parts HNO_3 + 1 part HCl to remove inclusions which can affect EPR results. For double loop testing wet grinding to 120 grit or 600 grit SiC paper was used.

Single and double loop measurements were performed according to Fig. 2, i.e., for single loop measurements the corrosion potential was measured for two minutes then a passivating potential of +200 mV(SCE) applied for two minutes. After this the potential was scanned back to the corrosion potential at a rate of 6 V/h. The current-potential curves were recorded and the charge passed during the reactivation scan integrated automatically. The charge associated with the passive current was subtracted, this having the same effect as zeroing the current integration at the start of the reactivation sweep as described in the recommended practice. P_a values were calculated using Equation (1) and ASTM grain sizes of 5.4 (as-delivered specimen and 1 hour at 620 °C) 5.7 (10 hours) or 5.8 (24 hours).

For double loop measurements the corrosion potential was measured for two minutes then the potential scanned at 6 V/h to +300 mV(SCE) and back. These results were evaluated both as an I_r/I_a ratio and as a P_a value obtained from integration of the reactivation scan. In all cases three measurements were made and averaged.

3.2 Studsvik, Sweden

An electrolyte volume of 700 ml was employed and dearated with nitrogen (8 l/h) for two minutes before and during testing. The reference electrode and counter electrode were standard calomel and graphite, respectively. Test temperatures of 30 °C and 35 °C were employed. Specimens were polished to 6 μm diamond paste followed by Al_2O_3 then masked using Glyptal Red Enamel (which was dried 30 minutes at room temperature + 30 minutes at 150 °C). An area of ~ 1.2 cm^2 of the outer pipe surface was, thus, exposed for testing. Single loop measurements were performed according to Fig. 2 with the difference that polarization to -500 mV (SCE) for 30 seconds was employed prior to measurement of the corrosion potential. The potentiostat employed was a PAR Model 173 and integration was performed using a PAR Coulometer model 179. P_a values were calculated using Equation (1) and ASTM grain sizes of 6.3 (as-delivered specimen), 6.0 (1 hour and 24 hours at 620 °C) or 5.5 (10 hours).

3.3 VTT, Finland

EPR measurements were performed using a field cell which contained a standard calomel reference electrode and a tubular platinum counter electrode, Fig. 3. About 10 ml of electrolyte was contained in a sponge inside the cell, testing was thus at ambient temperature (~ 20 °C) and in aerated conditions. Measurements were performed on the outer pipe surface of the specimens after polishing to 1 μm diamond paste and then etching for 30 seconds in 2 parts HNO_3 + 1 part HCl. Measurements were performed according to Fig. 2 with passivation at +200 mV(SCE), being maintained for two minutes or until the current density was lower than 10 μA/cm^2. A Wenking LB75L potentiostat with a Hewlett Packard 85 PC-control was employed and results evaluated according to Equation (1) with an ASTM grain size of 6.0. To expose the specific area of the test specimen precut pieces of masking tape, Nitto Tape 21, Genk, Belgium, were used.

3.4 ENEA, Italy

A test cell containing 600 ml of solution was employed, the same solution being used for three measurements then changed. A platinum counter electrode was employed and a saturated calomel reference electrode separated from the cell by a salt bridge with a Vycor tip. The temperature was maintained by means of an electrical heating mantle coupled to a thermoregulator and the solution was deaerated with nitrogen (150 cm^3/min) for one hour before and during testing. The EPR-test was conducted with a PAR Model 350 potentiostat. The results are average of three measurements.

The test specimens were machined into discs 2 - 4 mm thick and ~ 16 mm in diameter and a test area of 1 cm^2 with a surface finish of 3 µm was employed. The double loop EPR method (17) was used, with the corrosion potential first being monitored for 30 minutes. After this the potential was swept to +200 mV(SCE) held at this level for 2 minutes then scanned back to the corrosion potential. Two different potential scan rates of 6 V/h and 12 V/h were employed and results evaluated in terms of P_a values according to Equation (1).

3.5 CISE, Italy

Single loop measurements were performed according to Clarke's recommended practice (15) and Fig. 2 on specimens polished to 1 µm. The results are average of four measurements.

3.6 Temperature dependence of EPR measurements (IM, Sweden)

A similar electrochemical cell to that used for the round robin testing at IM was employed for single loop measurements to evaluate the temperature dependence of EPR measurements. Specimens were, however, instead machined to cylinders of 11 mm diameter, a wire spot welded to the reverse side and the whole assembly mounted in cold setting plastic so as to expose a circle of area ~ 1 cm^2 corresponding to the outer pipe surface. A Wenking POS 73 potentiostat was employed and the charge passed during the reactivation scan determined by integration of linear current-potential curves using a MOP image analyzer. EPR-measurements were performed at 10 °C, 20 °C, 30 °C and 40 °C.

The microstructures resulting from EPR testing were analyzed using an IBAS 2000 image analysis system. The total length of grain boundary attack was measured at a low magnification (giving a measuring frame size of 1 x 1 mm^2 or 512 x 512 $pixel^2$) after the width of the attacked regions had been reduced to one pixel. The width of the grain boundary attack was evaluated at higher enlargement (measuring frame 0.2 x 0.2 mm^2) by first measuring the total attacked area per frame then dividing this by the total grain boundary length determined in the same way as at low magnification. In both cases the results from five measuring frames were averaged. In addition the depth of grain boundary attack was determined manually at 1000x magnification using a Nikon light optical microscope with calibrated focussing.

3.7 EPR-round robin results

The results from the round robin testing are listed in Table 2 and typical microstructures after single and double

loop testing at VTT are shown in Figs. 4 and 5. All testing laboratories ranked the specimens in the same order and agreement between the different measurements is good.

The results of single loop EPR measurements on a larger number of specimens at temperatures from 10 °C to 40 °C are listed in Table 3 and plotted as a function of sensitization time in Fig. 6. From this it is apparent that EPR measurements saturate at the higher degrees of sensitization irrespective of testing temperature. The effect of temperature becomes more pronounced as the degree of sensitization increases since a 10 °C rise in temperature produces approximately a doubling of the P_a value. This effect may be rationalized in terms of an activation energy for dissolution during EPR measurements, evaluated from the Arrhenius plot in Fig. 7 as 67 ± 9 $kJmol^{-1}$. This may then be used to derive an equation for converting P_a values measured at a temperature T °C to P_a' values at 30 °C:

$$P_a' = P_a \exp \{ \frac{26.55(30-T)}{(273+T)} \} \qquad (3)$$

If Equation (3) is applied to the results from the round robin obtained at temperatures other than 30 °C, the figures in parentheses in Table 2 are obtained. These corrected values clearly then show much better agreement with the bulk of the measurements which were performed at 30 °C. This is shown in Fig. 8 where all the EPR measurements performed in the round robin are plotted as a function of sensitization time. Studsvik's measurements at 35 °C and VTT's measurements at 20 °C have been corrected to 30 °C and the charge in ENEA's measurements at 12 V/h doubled to compensate for the difference in time factor compared to the standard 6 V/h. If all these measurements are averaged, P_a values of 0.05 ± 0.04, 2.00 ± 1.30, 18.30 ± 3.60 and 25.47 ± 4.05 are obtained for the four round robin specimens (as delivered and furnace sensitized for 1 hour, 10 hours and 24 hours, respectively).

These standard deviations are only of the order of double those obtained by repeated testing at the same laboratory indicating the excellent reproducibility of EPR measurements in spite of marked differences in test procedures. It is also apparent from Fig. 8 that there is no clear systematic difference between test results, even if single and double loop testing is compared.

Additionally, IM studied the effects of surface finish on EPR results. Figure 9 shows that there is no systematic effect to be observed.

In order to find out if use of field cell causes different results as compared to normal polarization cell, VTT performed an additional test series presented in Table 4. The

same polarization instrument system was used and field cell was tested both with 0.01 N KSCN and 0.01 N NH_4SCN solutions at 20 °C and laboratory cell was used at 30 °C (0,01 N KSCN solution) both for test surface defined by tape and lacquer. When the field cell results are converted to 30 °C according to Equation (3) values obtained are lower than those obtained with the laboratory cell. The reason for this is not known, but it might be the difference in deaeration or the possibility that the wetted sponge does not have an even contact on the whole surface, e.g., due to gas bubbles. Also it is clear that defining of surface area with lacquer results in higher values, which probably is due to uncertainties in actual surface area, which with the tape is very reproducible. An example of surfaces after EPR-measurements with a tape is shown in Fig. 10. If one compares these laboratory cell results to Fig. 8 it is evident that the results agree very well.

The results of EPR measurements of IM at various temperatures in terms of both the dissolution charge and the P_a values, are presented together with the measured metallographic parameter in Table 3. The P_a values were calculated from the equations:

$$P_a = Q/GBA \quad (1)$$

$$GBA = A \cdot 5.09544 \times 10^{-3} \exp(0.34696X) \quad (2)$$

$$X = 3.2877 - 6.6439 (\log_{10} \bar{l}) \quad (4)$$

$$\bar{l} = \pi/2L_A \quad (5)$$

where Q is the charge passed (in C), GBA the grain boundary area (in cm^2), A the specimen area (in cm^2), X the ASTM grain size, $\bar{l}$ the mean linear intercept (in mm) and L_A the length of grain boundary per unit specimen area (in mm/mm^2). The latter parameter was taken from the length of attacked grain boundary in specimen 8 tested at 40 °C (Table 3) as practically all grain boundaries were attacked in this case. This gave an ASTM grain size of 6.0, which was in excellent agreement with measurements made according to the circular intercept procedure in the ASTM standard.

Equation (5) above suggests, however, a more direct and rigorous way of calculating P_a values than that given in Equations (1) and (2), namely

$$GBA = L_A Aw = \frac{\pi Aw}{2\bar{l}} = 1.57 \frac{Aw}{\bar{l}} \quad (6)$$

where w is the width of the attacked region at the grain boundary (assumed by Clarke et al. (15, 20, 13) to be 1

μm). This may be compared with evaluation of Equations (2) and (4) above which give

$$GBA = 1.63 \frac{Aw}{\bar{l}} \qquad (7)$$

if all quantities are expressed in the same units. The discrepancy is caused by equations (2) and (7) assuming a circular grain shape while equation (6) is a rigorous expression which makes no such assumption.

Since, however, the width of the attacked grain boundary region is seldom known and in addition is shown in Table 3 to deviate considerably from the value of 1 μm assumed by Clarke et al. (15, 20, 13), it would be preferable to eliminate this term and express the degree of sensitization as a Q_L value (charge normalized to grain boundary length)

$$Q_L = \frac{Q}{GBL} \qquad (8)$$

$$GBL = \frac{\pi A}{2\bar{l}} \qquad (9)$$

Thus P_a values (in Ccm^{-2}) would have to be multiplied by a factor of 0.0104 to convert them to the corresponding Q_L values (in Cm^{-1}).

The results of quantitative image analysis are listed in Table 3. In Figure 11 the length, width and depth of grain boundary attack are plotted as a function of both sensitization time and EPR testing temperatures. This indicates that the length of attacked grain boundary increases with an increasing degree of sensitization of the specimen but is relatively insensitive to testing temperature. The width and depth of attack are on the other hand governed by testing temperature and thus reflect dissolution kinetics rather than the sensitization state of the material being tested.

There has been considerable discussion about the underlying cause of grain boundary attack in EPR testing. Aho-Mantila et al. (18) observed prominent carbide particles in the attacked areas and thus reasoned that it was the Cr-depleted regions rather than the carbides themselves which initiated dissolution. The results presented in Table 3 and Fig. 11 clearly show the attacked width to be considerably greater than the typical width of the Cr-depleted zone (1). They are, however, consistent with the idea that a critical width of sufficient Cr-depletion is necessary to initiate

attack which then propagates into the surrounding undepleted material to an extent (width) governed by the kinetics of dissolution and, thus, temperature. This may be explained by the EPR testing conditions being sufficiently aggressive to allow propagation of already initiated attack into undepleted material but not to allow this material itself to depassivate.

Finally, Fig. 12 compares the measured depth of grain boundary attack to the expected depth calculated from the equation

$$d = \frac{QM}{lw\rho Fz} \qquad (10)$$

where Q is the dissolution charge, M the average atomic weight of the steel (55), l and w the length of width of grain boundary attack respectively, ρ the steel density (7860 kgm^{-3}), F Faraday's constant and z the average number of electrons involved in the dissolution of one metal atom (2.2). The results show generally good agreement, indicating the close relation between EPR microstructures and the measured charge.

3.8 Conclusions

1. EPR measurements provide a reliable, reproducible method of measuring the degree of sensitization of AISI 304 stainless steels.

2. Agreement between tests performed at different laboratories is good, indicating that surface preparation and testing procedure have only a small effect on EPR-results. However, test temperature, determination of ASTM grain size and definition of surface area are the major variables affecting the resuls, besides the DOS.

3. EPR results are strongly dependent on the testing temperature. Increasing the temperature increases the dissolution charge (Q) by an amount consistent with a dissolution activation energy of 67 ± 9 $kJmol^{-1}$. P_a values obtained at a temperature T °C may thus be converted to P_a at 30 °C using the Equation:

$$P'_a = P_a \exp\left\{\frac{26.55(30-T)}{(273+T)}\right\}$$

4. The degree of sensitization could also be expressed as a dissolution charge normalized to the grain boundary length and expressed as a Q_L value in Cm^{-1}

$$Q_L = \frac{\bar{Q}2\bar{l}}{\pi A}$$

where Q is the dissolution charge obtained from EPR measurements, l the mean grain boundary linear intercept length (used to evaluate ASTM grain size) and A the test specimen area. Q_L values may be converted to P_a values (e.g. assuming an attack width of 1 μm) in Ccm^{-2} by multiplying by a factor of 96.4.

5. With an increasing degree of sensitization a greater length of grain boundary is attacked in EPR testing. The width and depth of attack are not affected as these are governed by dissolution kinetics and thus testing temperature.

6. There is good quantitative agreement between the dissolution charges measured using the EPR technique and the dimensions of the grain boundary attack measured using image analysis.

4. MATERIAL CHARACTERIZATION

The circumferentially welded pipe specimen (Fig. 13) was of the same composition as the round robin material (see the control analyses in Table 1), and after welding it had been in service for 45 000 hours at 230 °C in Ringhals 1 BWR-plant. EPR measurements were first performed on both internal and external pipe surfaces in the heat affected zone, Lacomit lacquer being used after surface preparation to restrict the exposed specimen area to a circle of diameter 10 mm (0.79 cm^2) (IM) or 6 mm (0.28 cm^2) (VTT) tangential to the fusion line (Fig. 14). The two longitudinal sides of the weld specimen were then ground, polished and electrolytically etched in 10 % oxalic acid according to ASTM A 262 Practice A (at a current density of 1 Acm^{-2} for 90 seconds). The entire HAZ was then photographed. These photographs were used for IBAS image analysis of the oxalic acid etched structures (3). The more sensitized side of HAZ was then cut parallel to the fusion line into sections 1-2 mm thick (Fig. 14b) using a low speed diamond saw. EPR measurements were performed on both sides of these sections, the tested area being a circle of 6 mm diameter (0.28 cm^2) (both at IM and at VTT) tangential to the inner pipe surface (Fig 14b) and Lacomit lacquer again being used to mask the remaining specimen surface at IM. At VTT a precut tape was attached to the measured surface. Portions of the same sections were also used for the ATEM and TEM studies of carbide precipitates and chromium depleted zones (11).

4.1 Measurement of the DOS

The macrostructure of the welded specimen is illustrated in Fig. 15 and shows the weld to have been built up of at least four passes. The extent of sensitization in the heat affected zone is illustrated in Figs. 16 and 17, which show the sides of the weld after oxalic acid etching according to ASTM A262 Practice A and after Strauss test according to ASTM A262 Practice E, respectively. There is a clear band of sensitization (grain boundary attack) running parallel to the fusion line and adjacent to it; this is relatively narrow near the top of the weld where the material has only been affected by the final pass but it is much broader towards the inner pipe surface.

The results of the EPR measurements of different laboratories on the heat affected zone are listed in Tables 5-9; the measurements on the sectioned HAZ are also shown in Figs. 18 and 19 as a function of distance from the fusion line. An example of microstructures after single loop testing of the sections is illustrated in Fig. 20 and comparison with the oxalic acid etch structures showed somewhat larger standard deviation in this case than for the furnace sensitized material, this being a result of the less uniform sensitizing process. In both cases (single and

double loop) there is, however, a clear maximum amount of sensitization at 2 - 3 mm from the fusion line. This is in qualitative agreement with results reported in similar studies (22, 23).

It is instructive to compare the results of EPR measurements on the external and internal surfaces of the HAZ (Tables 5 and 7) with those on the transverse sections. It is clear that even measurements on the more heavily sensitized inner pipe surface do not reflect the full degree of HAZ sensitization; a P_a value for the inner pipe surface of 16.7 Ccm^{-2} may be compared with a maximum of 33.5 Ccm^{-2} for the transverse sections measured at IM. The corresponding values of IM for the i_c/i_a ratio in double loop measurements is 32.14 x 10^{-3} and 83.3 x 10^{-3}, respectively. The EPR measurements on the internal and external pipe surfaces may also be compared with the acceptance limits of Clarke et al. (15, 20): 2 Ccm^{-2} on the outer surface for base material (considered conservative) or 5 Ccm^{-2} on the inner surface proposed for weldments. Although the outer (practically accessible) surface of side A with an IM P_a value of 1.97 Ccm^{-2} fulfills these criteria, the inner surface (16.7 Ccm^{-2}) clearly does not. This is a serious discrepancy, particularly in view of Clarke's et al. (15) observation that pipes with an inner surface P_a value above 12 Ccm^{-2} failed by intergranular stress corrosion cracking, and underlines the significance of welding practice on sensitization and, thus, IGSCC.

The results of IBAS image analysis of the oxalic acid etch structures on the longitudinal sections of the weld have been reported in detail elsewhere (3). For purposes of comparison, the length fraction of ditched grain boundaries is shown as a function of distance from the fusion line in Table 10 and Fig. 22. From these it is apparent that there is a considerable difference in the degree of sensitization on the two sections, i.e. along the length of the weld. This inherent variation in the amount of sensitization can largely explain the relatively high standard deviations of the EPR measurements, which are, thus, due to variations in the material tested rather than to poor reproducibility of the test method, per se. Also shown in Table 10 and Fig. 22 is the standard classification of etch structures into step (unsensitized) dual and ditch (some grains completely surrounded by grain boundary attack). The transition between ditch and dual structures appears to correspond to ~ 50 % grain boundary ditching; the transition to a step structure occurs at < 5 %.

Fig. 23 shows a comparison between the single loop, double loop and oxalic acid testing of the weld HAZ. This indicates that although the correlation between double and single loop EPR measurements is very good, the double loop curve and maximum are systematically shifted somewhat closer towards the fusion line. The reason for this is not

clear but the difference is so small as to probably lack practical significance. Comparing the EPR measurements with the oxalic acid etch results showed good correlation although the latter gives a broader maximum with a maximum degree of sensitization at 3 - 4 mm from the fusion line (c.f. 2 - 3 mm for the EPR measurements). This may partly be explained by the different areas investigated in the two cases: EPR measurements were performed on a circle of diameter 6 mm tangential to the inner pipe surface (Fig. 14b) while analysis of oxalic acid etch structures was performed only at 3 mm from the inner pipe surface on the sides of sections cut from the weldment. A second contributing factor may be that attack in the oxalic acid test initiates at carbides (18), which were observed as far away from the fusion line as 8.5 mm in ATEM-study, while the initiation of attack in EPR-testing is associated with chromium depletion which according to the ATEM investigations (11) was almost negligible 5 mm from the fusion line. Also apparent from Fig. 23 is the steeper fall-off of sensitization as measured by the oxalic acid test; this is in line with Clarke's et al. observation (15) that EPR measurements give a better differentiation than oxalic acid etch structures at moderate degrees of sensitization.

Fig. 23 nevertheless shows that oxalic acid etching also gives a quantifiable measure of the degree of sensitization if the length fraction of grain boundary ditching is measured rather than the standard step/dual/ditch classification being employed. It may incidentally be seen from Fig. 23 that the transition from a step to dual structure, considered to represent "discernible intergranular precipitation" corresponds roughly to a P_a value of 2 - 4 Ccm^{-2} or an i_c/i_a ratio of 0.001 - 0.002. This is comparable with other reported results (16, 17).

The correlation with single and double loop EPR-results obtained at IM indicates a very good correlation, Fig. 24. Reproducibility of the two methods was similar in contrast to Mijidi and Streicher (17), who obtained better reproducibility for the DL-method. This suggests that practically easier DL-method could satisfactorily be applied to field or laboratory testing.

No comparison is possible here with the results of other forms of intergranular corrosion testing (e.g. ASTM A262 Practices B-E), since they are not quantitative. However, it can be seen from Figure 17 that near the inner surface of the pipe the attack in the Strauss test extends to about 4 - 5 mm from the fusion line and that near the outer surface of the pipe no attack is present. Previously reported results (15) suggest that both EPR and oxalic acid testing show saturation at very high degrees of sensitization (unlike the boiling acid tests) and are thus most suitable for measuring moderate amounts of sensitization.

It is, however, such moderate degrees of sensitization that most commonly occur, for example, as a result of welding.

4.2 Electron Microscopy

The pipe weld of stainless steel (SS 2333) which had been in service in Ringhals 1 reactor for 45 000 hours at 230 °C was examined with respect to chromium depletion at grain boundaries using analytical transmission electron microscopy (ATEM). Specimens from the heat affected zone with different well defined distances from the fusion line were cut out for this study and for correlation with corrosion tests (Fig. 14b). Chromium depleted zones have been observed at grain boundaries in the vicinity of chromium carbides. Both the degree of depletion and the size of the carbides were greatest close to the fusion line. A high level of depletion was measured at grain boundaries between carbide particles, 1.9 mm from the fusion line, and this decreased to almost bulk value at a distance of 4.9 mm from the fusion line.

At the distance of 1.9 mm from the fusion line the lowest measured Cr-content at the grain boundary was 13.5 % Cr. On one side the Cr-profile was very steep (only 25 nm) while on the other side it was rather sloping (about 120 nm) showing, thus, a highly asymmetric profile, Fig. 25a. At this distance the particle size was about 100 nm.

At the distance of about 3.5 mm from the fusion line the carbide size was about 50 nm and the Cr-depletion profiles were still asymmetric, Fig. 25b. At this distance the Cr-depleted zone was fairly similar to the previous case, but it is slightly narrower.

At the distance of about 4.9 mm from the fusion line, Fig. 26a, the particles were only about 25 nm in size. Only at a few locations between carbides at the grain boundaries it was possible to detect any Cr-depletion. Further away from the fusion line no Cr-depletion was observed and also only a few carbide particles were present, there.

The existence of asymmetric Cr-profiles has been observed by Hall and Briant (24) in austenitic stainless steels even after ageing at 700 °C. This, and the pyramid form of the particles indicates that they have grown discontinuously. This effect is most evident at the distance of about 2 mm from the fusion line. If Ringhals 1 material is compared to the reference material (only welded) it is evident that the Cr-depleted zone is more than double as wide as in the reference material and also its asymmetric form is much more evident, which may indicate that low temperature sensitization has taken place even at as low temperature as 230 °C. The fact that the C-content of the reference material was 0.01 % C lower, Table 1, however, makes the quantitative analysis difficult.

The compositions of the particles were also analyzed from replicas, Table 11. It can be seen that $M_{23}C_6$ carbides have a very high Cr-content at the austenite grain boundaries, but much lower Cr-content at austenite/ferrite phase boundaries present near the fusion line.

Asymmetric chromium concentration profiles, normal to the grain boundaries as well as the shape and orientation of the carbides indicates grain boundary migration due to discontinuous precipitation of $M_{23}C_6$ carbides, Fig. 27. Similar structures and asymmetrical profiles were measured 2 mm from the fusion line in a reference steel (Table 1) which had not been exposed to low temperature treatment after welding (22). Also in this case is the Cr-profile slightly asymmetric, Fig. 26b, like in the Ringhals 1 weld. The particles here were smaller corresponding to about 0.01 % lower carbon content and also the width of the zone is less than half of that in the Ringhals 1 weld. Any possible chromium depletion, due to the low temperature sensitization (LTS) at 230 °C is apparently small and can not be unambiguously detected using the present ATEM-technique.

To determine the size and the type of the grain boundary carbides the JEOL JSEM 200 transmission electron microscope was utilized at VTT. After the EPR and DL-EPR measurements the specimens were first mechanically polished to the thickness of 0.15 mm and then finished by low-temperature electropolishing technique employing the "window-method" and an electrolyte of 30 percent HNO_3 in ethanol.

The TEM studies clearly indicate that the size of the grain boundary carbides decreases when the distance from the fusion line increases (Fig. 28). In the first specimen, next to the fusion line, the grain boundary carbides are only locally present and large (diameter 150 - 200 nm) as shown in Fig. 28. Further away from the fusion line, the carbide size decreases, but their number increases (Table 12 and Figs. 30 - 34). At the distance of 5.5 mm from the fusion line, the carbide size varies markedly and a number of the smallest carbides may have been inadvertently omitted from counting resulting in a larger average size and smaller number than actually present, Fig. 32. At the distance of 7.0 mm from the fusion line it is almost impossible to count the carbides due to their small size, Fig. 33. The carbide structures in the reference specimen are presented in Fig. 35 for distances of 0.7 mm and 2.7 mm from the fusion line. It can be seen that there is a dense carbide distribution on these grain boundaries.

According to the TEM analysis of the grain boundary carbides, they are of the type $M_{23}C_6$.

4.3 Correlation of DOS to TEM/ATEM investigations

Analytical transmission electron microscopy and TEM studies to determine the degree of carbide precipitation and chromium depletion in the HAZ of the welded specimens showed that carbides had grown via a discontinuous precipitation mechanism (grain boundary migration). There was no clear evidence that marked low temperature sensitization had occurred during service, the observed features being most probably mainly a result of weld sensitization. The latter is not unexpected as the service temperature was relatively low, 230 °C. The observed variation in carbide morphology and chromium depletion as a function of distance from the fusion line shows a good correlation. It is, however, also clear that there is not an exact correspondence between EPR measurements and the degree of chromium depletion, or between oxalic acid etching and carbide precipitation. While the EPR maximum coincides with the lowest grain boundary chromium level, both the single and double loop measurements indicate a considerable degree of sensitization even at ~ 5 mm from the fusion line even though chromium depletion is negligible. Oxalic acid etching exhibits a broader sensitization peak at ~ 2 - 6 mm from the fusion line. This is in reasonable agreement with the results in Table 12 which show a maximum carbide size at 2.5 mm from the fusion line, but a maximum number at 5.5 mm. The distribution of carbides, i.e., amount of grain boundaries decorated with carbides would, however, be expected to show better correlation because the carbides merely act as the initiation point for attack which subsequently spreads over a much wider area around the grain boundary.

It is also instructive to compare the sensitization curves of Fig. 23 with the behavior predicted from a knowledge of precipitation kinetics and calculation of heat flow through the HAZ during welding. The results of such calculations performed by Aaltonen et al. (19) for AISI 304 steel welded with different input energies are shown in Fig. 36. This indicates that it is material ~ 1 - 3 mm from the fusion line, which has a peak temperature in the range 500-800 °C and has, thus, been exposed for the longest times to the temperatures required for carbide precipitation. To obtain an exact correlation it is naturally necessary to take into account other parameters such as the effect of several weld passes, carbide nucleation time and the effect of stresses in the HAZ on precipitation kinetics. There is nevertheless a good qualitative agreement between the predictions of Fig. 36 and the sensitization curves of Fig. 23.

4.4 Conclusions

In the case of the welded specimen, EPR measurements on the transversely sectioned HAZ showed a maximum degree of

sensitization at 2 - 3 mm from the fusion line. This is in reasonable agreement with IBAS image analysis of oxalic acid etched structures, which showed a sensitization maximum at 3 - 4 mm from the fusion line, and ATEM investigations which showed a maximum amount of carbide precipitation and grain boundary chromium depletion at ~ 2 mm from the fusion line. EPR measurements performed on the internal and external pipe surfaces before sectioning the HAZ suggest that care should be exercised in applying general acceptance limits to welded structures: while the external surface showed an acceptably low level of sensitization by the use of multipass welding meant that the inner surface was heavily sensitized.

The results of this study do not unambiguously indicate the increase of DOS of a sensitized zone in the HAZ of AISI 304 Type stainless steel during reactor operation as a result of LTS. After welding, the degree of sensitization is low, but it can increase during operation due to LTS. During LTS no new carbides are nucleated. The development of a sensitized microstructure in LTS includes two stages: (i) the nucleation and initial growth during welding and the geometric growth during which the number and shape of carbides remains constants, and (ii) the coarsening stage during which the carbide growth occurs at the expense of the neighboring carbides and the geometric shape is lost. The change can be explained by the pronounced effect of grain boundary diffusion of chromium at low temperatures and the growth of $M_{23}C_6$ grain boundary carbides involving grain boundary migration.

5. STRESS CORROSION TESTING

In laboratory tests a critical corrosion potential for IGSCC in BWR environment has been observed. This critical potential (E_{σ}), however, depends on the metallurgical parameters, the degree of sensitization (DOS), the temperature, and on the conductivity and impurity content of the environment.

In this study slow strain rate testing (SSRT) and multipotential testing with U-bend specimens was performed on pipe weld sections taken from Ringhals 1 to measure materials susceptibility to IGSCC. The weld had been in service for 45 000 h at 230 °C. The degree of sensitization and carbide structure in the heat affected zone (HAZ) of the weld was presented in Chapter 4.

5.1 Slow strain rate tests

Smooth tensile specimens, Fig. 37, with a gauge length of 25 mm were used in SSRT tests. The specimens were manufactured with the intention of having the HAZ located in the middle of the specimen gauge length.

Specimens for multipotential testing were manufactured according to Fig. 38. The HAZ of the weld was sliced by spark cutting method and slices with certain distance from the weld fusion line were bent to form U-bend specimens.

Prior to testing the specimens for both tests were wet-polished with 600 mesh SiC-paper, the dimensions were measured, and the specimens were ultrasonically cleaned in acetone and alcohol.

A total of four specimens from the pipe weld were tested according to Table 12. The SSRT-tests were performed according to the following procedure. The unloaded specimen was exposed to deoxygenated water during heating. Then oxygenated water was added. After a pre-exposure period at established environmental conditions the specimen was preloaded (in the case of testing in air-saturated water) and the straining was started. The straining continued to failure and the specimen was finally examined in a scanning electron microscope (SEM). The SSRT tests at controlled electrode potential were performed in high purity water at 250 °C. The inlet conductivity of the water was less than 0.08 µS/cm. The specimens were galvanically insulated from the autoclave.

The tests were made in a 0.8 l autoclave with a flow rate of 5 l/h. Internal silver chloride reference electrodes were used (Ag, AgCl/0.01 m KCl). The potential of the specimen was controlled by means of a closed-loop oxygen dosage system. The test set-up is shown in Fig 39. The

elongation rate was 5.8 x 10^{-4} mm/min and the specimens were not preloaded.

The SSRT tests in air-saturated deionized water at 250 °C were made in a 37 l autoclave with a flow rate of 10 l/h. The specimens were galvanically insulated from the autoclave. The elongation rate was 7.5 x 10^{-5} mm/min and the specimens were preloaded.

5.2 Multipotential tests with U-bend specimens

After cutting the U-bends from the welded pipe (Fig. 38) they were placed in the test rig (Fig. 40). The test rig contained five different SS rings each having five U-bend specimens taken from different distances from the fusion line. The five rings with specimens were polarized to different test potentials. In the multipotential method the ring 1 remains at its free corrosion potential which is controlled by a potentiostat. This means that the potential drop between the reference electrode and the ring 1 is near zero. Other potentials are created between the ring 1 and the other rings by a current supply and external resistors. After the test the U-bend specimens were studied by SEM.

Multipotential tests were conducted in a static autoclave at 288 °C. The autoclave was filled with deionized water with low conductivity. In the beginning of the test the water was oxygen rich and the corresponding corrosion potential of autoclave internals was ~ -200 mV(SHE). Within a couple of days the oxygen was consumed and the potential of the internals decreased below -500 mV(SHE).

5.3 Test results

The results from the SSRT are given in Table 14 and in Figs. 41 and 42. Environmental data during the tests are given in Table 15.

The specimens NKA 2 and 3 that were tested at ~ -250 and ~ -200 mV(SHE), respectively, did not show any IGSCC. The specimens NKA 4 and 5 that were tested in air-saturated water showed an entirely intergranular fracture surface, Fig. 43.

The static multipotential exposure at 288 °C was conducted first for 50 days at following potentials: -300, -275, -250, -225 and -200 mV(SHE). When the inspection with optical microscopy after this period revealed no cracking the test potentials were changed as follows: -250, -200, -150, -100 and 0 mV(SHE). The second exposure lasted 60 days. The observed crackings are summarized in Table 16.

IGSCC was observed in specimens taken at the distance of 3.5 and 6 mm from the fusion line corresponding to the high DOS, according to Fig. 18. The IGSCC took place at -0 and

-100 mV(SHE). Cracking observed in SEM was intergranular and appeared always near the other edge of the bend specimens corresponding to original inner surface of the pipe. In the same specimens minor pitting was also observed.

In previous studies with the same SSRT experimental set-up the critical potential for IGSCC of sensitized austenitic stainless steel of type SS 2333 has been determined to be in the range -250 to -300 mV(SHE) (26). This critical potential value was determined by SSRT of smooth specimens at a nominal strain rate of 4×10^{-7} s^{-1} and a heavily furnace sensitized material was used. It was therefore anticipated that the welded specimen tested at -200 mV(SHE) in this study should show IGSCC after SSRT. The reason why IGSCC did not occur could either be a result of lower DOS or water chemistry improvements in the laboratory after the previous work was performed.

The degree of sensitization in the material used in this study was high. The specimens for SSRT were cut from the welded pipe, with the HAZ located within the specimen gauge length, and the most sensitized part of the pipe was located on or near the inner surface of the pipe wall. This most sensitized area was, however, removed during specimen manufacturing. The actual sensitization in the SSRT specimens was therefore less than the P_a-values measured in Fig. 18.

It should also be noted that the strain rate during SSRT of a welded specimen is not well defined. Large variations can occur along the gauge length, which can also effect the initiation of IGSCC during the test.

Both test methods revealed IGSCC at the highest potential corresponding oxygen saturated conditions. Test specimens used in the multipotential test showed IGSCC also at a lower potential (-100 mV(SHE)). At this potential no SSRT-tests were performed. No cracking was observed at -200 mV(SHE) independent of test method. Multipotential testing showed cracking consistent with the location of the highest DOS near the original inner surface which was not included in SSRT specimens. The water chemistry during multipotential testing excluding oxygen content was not well controlled because of the static testing method employed. In the future the SSRT specimen manufacturing method should be improved so that the inner surface of the original pipe can be tested. In multipotential testing the water chemistry control should be improved by using autoclaves with water circulation and purification.

5.4 Conclusions

SSRT of specimens from a pipe weld removed from Ringhals 1 in high purity water at 250 °C at controlled electrode potentials of -250 and -200 mV(SHE) did not result in any

IGSCC. Testing in air-saturated water gave entirely intergranular fracture surfaces.

Testing with multipotential method showed IGSCC at 288 °C at potentials 0 mV and at -100 mV(SHE). The fastest cracking was observed in specimens taken from the distance between 3.5 - 6 mm from the fusion line, where the DOS is high but not at the maximum.

6. GENERAL CONCLUSIONS

The main conclusions of this NKA 530 study on "Intergranular stress corrosion", where an austenitic stainless steel pipe (SS 2333) after exposure of 45 000 hours in the Ringhals 1 BWR-plant at 230 °C was carefully examined, are

1. EPR measurements performed on furnace and weld sensitized AISI 304 stainless steel (0.052 % C) using both the single and double loop techniques showed that reproducibility of both methods is similar, and correlation between them is good.

2. In the case of the welded specimen, EPR measurements on the transversely sectioned HAZ showed a maximum degree of sensitization at 2 - 3 mm from the fusion line. This is in reasonable agreement with ATEM investigations which showed a maximum amount of carbide precipitation and grain boundary chromium depletion at ~ 2 mm from the fusion line.

3. EPR measurements performed on the internal and external pipe surfaces before sectioning the HAZ suggest that care should be exercised in applying general acceptance limits to welded structures: while the external surface showed an acceptably low level of sensitization, the inner pipe surface was heavily sensitized.

4. Agreement between EPR-tests performed at different laboratories is good, indicating that surface preparation and testing procedure have only a small effect on EPR-results; the major variables besides the DOS being ASTM-grain size, defining of measuring area, and test temperature.

5. EPR results are strongly dependent on the testing temperature. Increasing temperature increases the dissolution charge (Q) by an amount consistent with a dissolution activation energy of 67 ± 9 $kJmol^{-1}$. P_a values obtained at a temperature T °C may, thus, be converted to P_a at 30 °C using the equation

$$P'_a = P_a \exp \{ \frac{26.55(30-T)}{(273+T)} \} \qquad (1)$$

6. Existence of low temperature sensitization (LTS) could not be unambiguously proven in the studied pipe weld.

7. SSRT tests of specimens from a pipe weld from Ringhals 1 in high purity water at 250 °C at controlled electrode potentials of -250 and -200 mV(SHE) did not result in IGSCC. Testing in air-saturated water gave entirely intergranular fracture surfaces.

8. SCC testing with multipotential method showed IGSCC at 288 °C at potentials 0 mV and at -100 mV(SHE). The fastest cracking was observed in specimens taken from the distance between 3.5 - 6 mm from the fusion line.

7. R E F E R E N C E S

7.1 Reports from this study

1. Lehtinen, B.
Kromutarmning i korngränser invid svetsar i rostfria rör som varit i drift i Ringhals 1.
Institutet för Metallforskning, IM-2107.
Stockholm, juli 1986.

2. Jargelius, R.F.A.
Application of the EPR technique to assess the degree of sensitization in a Type 304 stainless steel.
Institutet för Metallforskning, IM-2276.
Stockholm, oktober 1987

3. Komenda, J., Jargelius, R.
A quantitative metallographic assessment of the degree of sensitization across a 19Cr10Ni stainless steel weldment.
Institutet för Metallforskning, IM-2275.
Stockholm, February 1988.

4. Berglund, T.
Korngränsfrätningsprovning av svetsfog och motsvarande grundmaterial från Ringhals 1.
Studsvik Energiteknik AB, EX-87/1.
Nyköping, januari 1987.

5. Svensson, B.-M.
EPR test of SS steel 2333 from Ringhals 1 in furnace sensitized and weld sensitized condition.
Studsvik Energiteknik AB, EX-88/16.
Nyköping, 1988.

6. Hertzman, S., Jargelius, R.F.A., Symniotis-Barrdahl, E.
Evaluation of the temperature dependence of EPR-measurements of the degree of sensitization in 304 stainless steel using quantitative metallography.
Institutet för Metallforskning, IM-2421.
Stockholm, 1989.

7. Molander, A.
Slow strain rate testing of welded material from Ringhals 1.
Studsvik Energiteknik AB, EX-88/31.
Nyköping, 1988.

8. Lehtinen, B.
Kromutarmning i korngränser invid svetsar i rostfria rör.
11. Nordiske Korrosjonsmøte. NKM 11. Stavanger 19. - 21. juni 1989.

9. Jargelius, R.F.A., Symniotis-Barrdahl, E., Aaltonen, P., Hänninen, H., Berglund, T., Elektrokemisk karakterisering av sensibilisering i SS 2333 (typ 304) Rostfritt stål. 11. Nordiske Korrosjonsmøte. NKM 11. Stavanger 19. - 21. juni 1989.

10. Aaltonen, P., Molander, A. Critical potential for intergranular stress corrosion cracking of austenitic stainless steel. 11. Nordiske Korrosjonsmøte. NKM 11. Stavanger 19. - 21. juni 1989.

11. Hänninen, H., Aaltonen, P., Jargelius, R.F.A., Molander, A. Intergranular stress corrosion cracking on austenitic stainless steels. 11. Nordiske Korrosjonsmøte. NKM 11. Stavanger 19. - 21. juni 1989.

7.2 Other references

12. Cihal, V., Desestret, A. et al. Tests d'etude et d'evaluation de la sensibilité inoxydables a la corrosion intergranulaire. 5th European Corrosion Congress, 24 - 28 Sept. 1973, Paris.

13. ASTM Committee G-1 on Corrosion of Metals. Standard electrochemical potentiokinetic reactivation (EPR) test method for detecting sensitization of AISI-304 and 304L stainless steels. 1989. In preparation.

14. Akashi, M., Kawamoto, T. Umemura, F. Boshoku Gijutsu Corrosion Engineering 29, 1980. 163.

15. Clarke, W. L., Cowan, R. L., Walker, W. L. Comparative methods for measuring degree of sensitization in stainless steel. ASTM STP 656 "Intergranular corrosion of stainless alloys", 1978, 99 - 132.

16. Majidi, A. P., Streicher, M. A. Potentiodynamic reactivation method for detecting sensitization in AISI 304 and 304L stainless steels. Corrosion 40:8, 1984. 393 - 408.

17. Majidi, A. P., Streicher, M. A. The double loop reactivation method for detecting sensitization in AISI 304 stainless steels. Corrosion 40:11, 1984. 584 - 593.

18. Aho-Mantila, I., Aaltonen, P., Hänninen, H.
Intergranular corrosion testing of austenitic stainless steels.
Technical Research Centre of Finland, VTT-MET-B26
Espoo, Finland, 1981.

19. Aaltonen, P., Aho-Mantila, I., Hänninen, H.
Electrochemical methods for testing the intergranular corrosion susceptibility of stainless steels.
Corrosion Science, 23:4, 1983, 431 - 440.

20. Clarke, W.L.
The EPR method for the detection of sensitization in stainless steels.
NUREG/CR-1095 GEAP-2488, 1981.

21. Cowan, R. L., Tedmon, C. S.
Intergranular corrosion in iron-nickel-chromium alloys.
Advances in Corrosion Science and Technology,
Vol. 3, (Eds. M.G. Fontana and R.W. Staehle)
Plenum, 1973.

22. Hänninen, H. et al.
Material characterization of AISI 304 steel pipe welds in TVO I shutdown cooling and cleanup system.
Industrial Power Company Ltd. (TVO) and Technical Research Centre of Finland (VTT), Final report,
October 1983.

23. Aho-Mantila, I., Aaltonen, P., Kekkonen, T., Hänninen, H.
Electrochemical reactivation tests for evaluating the susceptibility to intergranular corrosion in Fe-Cr-Ni alloys. 8e congrés européen de corrosion.
Vol 2: Communication posters, European Federaton of Corrosion, Paris, 1985.

24. Hall, E.L., Briant, C.L.
Chromium depletion in the vicinity of carbides in sensitized austenitic stainless steels.
Met. Trans 15A, 1984, 793 - 811.

25. Kekkonen, T., Aaltonen, P., Hänninen, H.
Metallurgical effects on the corrosion resistance of a low temperature sensitized welded AISI Type 304 stainless steel.
Corrosion Science, 25:8/9, 1985, 821 - 836.

26. Rosengren, A., Rosborg, B.
Critical potential for IGSCC of type 304 stainless steel in high purity water at 250 °C.
Proc. Inter. Symp. on Environmental Degradation of Materials in Nuclear Power Systems - Water Reactors, NACE, Houston, 1984, 592 - 603.

TABLE 1 Chemical composition of the AISI 304 steel (SS 2333, Sandvik charge 4-31099).

	C	Si	Mn	P	S	Cr	Ni	Mo
				%				
Charge analysis	0.052	0.55	1.23	0.017	0.011	18.7	9.5	0.39
Control analysis (side A of weld)	0.054	0.64	1.29	0.024	0.009	18.56	9.33	0.41
Control analysis (side B of weld)	0.055	0.72	1.23	0.019	0.009	18.11	9.22	0.16
Reference material for ATEM	0.043	0.38	1.82	0.023	0.015	19.1	10.2	0.10

TABLE 2 Results of round robin testing of furnace sensitized specimens expressed as P_a values in C/cm^2. Unless otherwise specified measurements were performed at 30 °C with a scan rate of 6 V/h. Specimen surface preparation is indicated in parentheses.

	Sensitisation time at 620°C			
Laboratory and testing method	0 hours	1 hours	10 hours	24 hours
IM-single loop (1 μm polished)	0.08±0.05	1.54±0.29	16.41±0.75	28.15±1.97
IM-single loop (1 μm+etched)	0.00±0.00	1.60±0.23	15.29±2.14	19.28±1.19
IM-double loop(600 grit SiC)P_a $(I_r/I_a)\times10^{-3}$	0.01±.0.01 (0.1±0.1)	0.59±0.17 (6.5±1.4)	12.85±2.24 (161.2±34.2)	20.74±2.11 (253.3±9.1)
IM-double loop(120 grit SiC)P_a $(I_r/I_a)\times10^{-3}$	0.01±0.00 (0.1±0.0)	0.59±0.14 (5.5±1.4)	15.82±1.50 (163.5±17.5)	21.23±1.19 (220.5±25.3)
Studsvik-single loop (Al_2O_3)	0.05	1.5	20	29
Studsvik-single loop (Al_2O_3) 35°C (corrected to 30°C)	0.07 (0.05)	3 (1.95)	36 (23.4)	40 (26)
VTT- single loop (1 μm+etch) 20°C (corrected to 30°C)	0.5±0.00 (0.12)	2.05±1.88 (5.07)	9.20±1.07 (22.8)	12.04±0.51 (29.80)
ENEA-double loop (3μm)	0.09±0.02	2.97±0.46	22.2±2.1	30.7±0.46
ENEA-double loop (3μm) 12V/h (x2 to correct for time factor)	0.021 (0.042)	0.91 (1.82)	8.24 (16.48)	11.9 (23.8)
CISE-single loop (1μm)	0.07±0.02	2.36±0.38	17.71±0.91	25.98±5.67

TABLE 3 Results of single loop EPR measurements at 10 - 40 °C on specimens furnace sensitized various times at 620 °C and image analysis of the resulting microstructures.

Spec.no.	Sensitis. time(h)	Testing temp.(°C)	Charge(C)	P_a(C/cm²)	Length ($\times 10^{-3}\mu m/\mu m^2$)	Width (μm)	Depth (μm)
1	0	10	0	0	0	0	0
		20	0	0	0	0	0
		30	0	0	0	0	0
		40	0	0	0	0	0
2	0.5	10	0.006	0.15	1.11	0	0
		20	0.017	0.43	0.43	3.43	1.31
		30	0.039	0.98	0.80	3.78	1.61
		40	0.125	3.15	1.68	3.18	2.12
3	1	10	0.0079±0.0010	0.20	1.14	2.52	0.87
		20	0.0198	0.50	0.76	3.04	1.35
		30	0.085	2.14	1.61	4.52	1.62
		40	0.179±0.030	4.51	2.10	4.85	1.94
4	3	10	0.057	1.44	14.26	1.41	0.53
		20	0.105	2.65	10.71	2.02	1.52
		30	0.459±0.024	11.57	30.30	3.82	1.65
		40	0.849	21.40	21.52	4.43	2.11
5	6	10	0.09	2.27	27.25	1.66	0.63
		20	0.262	6.60	25.22	2.07	1.75
		30	0.639±0.010	16.10	33.96	3.55	1.94
		40	1.067	26.89	29.54	3.88	2.2
6	9.5	10	0.123	3.10	31.63	1.51	0.68
		20	0.379	9.55	33.47	2.25	1.81
		30	0.85±0.082	21.42	37.54	3.9	1.96
		40	1.90	47.89	36.95	4.07	2.26
7	16	10	0.203	5.12	37.17	1.57	0.65
		20	0.374	9.43	37.91	2.16	1.54
		30	1.001	25.20	38.89	3.19	2.06
		40	1.76	44.36	40.98	4.26	2.35
8	24	10	0.175	4.41	36.89	1.79	0.81
		20	0.316	7.96	36.56	2.22	1.75
		30	0.934±0.086	23.54	39.36	3.48	1.93
		40	2.03	51.16	40.14	4.2	2.42

TABLE 4 VTT test results to compare KSCN- and NH_4SCN-solutions with the field cell and comparison to laboratory cell results at 30 °C in KSCN-solution using same polarization instrumentation.

	Testing method			
Sensitization	Field Cell 0.01 N KSCN	Field Cell 0.01 N NH_4SCN	Lab. test Area selective tape	Laquer area selection
	20 °C	20 °C	30 °C	30 °C
Solutions annealed	0.026	0.014	0.043	0.028
(corrected to 30 °C)	(0.063)	(0.034)		
1 h/620 °C	0.89	0.77	2.96	3.97
(corrected to 30 °C)	(2.20)	(1.89)		
10 h/620 °C	6.00	6.21	19.49	24.63
(corrected to 30 °C)	(14.86)	(15.38)		
24 h/620 °C	7.15	8.73	25.81	29.5
(corrected to 30 °C)	(17.69)	(21.62)		

TABLE 5 Results of single loop EPR measurements on inner and outer pipe surfaces (polished to 1 µm and etched in HCl/HNO_3) at IM and at VTT (field cell at RT and ASTM grain size 6.0).

Specimen	ASTM grain size (IM)	IM average (±SD) P_a (Ccm^{-2})	VTT P_a (Ccm^{-2})
AO (outer)	4.7	1.97 ± 0.5	0.8
AI (inner)		16.7 ± 3.1	4.7
BO (outer)	3.2	0.09 ± 0.03	0.07
BI (inner)		4.41 ± 0.82	3.2

TABLE 6 Results of single loop EPR measurements at IM on the sectioned side A of the HAZ (polished to 1 μm). ASTM grain size 4.7.

Specimen	Distance from fusion line (mm)	Average P_a (± S.D) (Ccm^{-2})
2B	15.70	0.73 ± 0.31
A	15.13	0.62 ± 0.27
3B	14.58	1.21 ± 0.35
A	12.93	0.80 ± 0.25
4B	12.36	1.24 ± 0.71
A	11.45	1.04 ± 0.29
5B	10.97	0.69 ± 0.11
A	9.84	0.74 ± 0.16
6B	9.45	1.11 ± 0.21
A	8.27	2.00 ± 0.38
7B	7.89	2.75 ± 0.08
A	6.83	4.70 ± 0.75
8B	6.20	12.57 ± 1.68
A	5.07	23.45 ± 5.53
9B	4.57	21.91 ± 2.70
A	3.86	25.76 ± 5.60
10B	3.13	33.55 ± 2.83
A	2.27	32.82 ± 2.94
11B	1.46	29.02 ± 4.24
A	0.37	14.17 ± 1.75

TABLE 7 Results of double loop EPR measurements on inner and outer pipe surfaces at IM and at VTT (field cell at RT).

Specimen	IM i_c/i_a ($x10^{-3}$) (±SD)	VTT, i_c/i_a ($x10^{-3}$)
AO (outer)	2.5 ± 0.15	1.6
AI (inner)	32.4 ± 3.3	32.0
BO (outer)	1.6 ± 0.7	1.3
BI (inner)	7.6 ± 4.4	30.0

TABLE 8 Results of double loop EPR measurements on the sectioned side A of the HAZ at IM.

Specimen	Distance from fusion line (mm)	Average i_c/i_a ($x10^{-3}$) (±S.D)
2B	15.70	2.5 ± 0.9
A	15.13	2.2 ± 1.9
3B	14.58	1.2 ± 0.0
A	12.93	1.3 ± 0.0
4B	12.36	1.2 ± 0.1
A	11.45	1.3 ± 1.0
5b	10.97	0.9 ± 0.1
A	9.84	1.5 ± 0.5
6B	9.45	1.2 ± 0.2
A	8.27	1.7 ± 0.1
7B	7.89	4.3 ± 3.1
A	6.83	8.2 ± 3.5
8B	6.20	15.7 ± 1.0
A	5.07	36.4 ± 4.0
9B	4.57	55.4 ± 7.6
A	3.86	73.2 ± 11.2
10B	3.13	68.9 ± 5.6
A	2.27	83.3 ± 15.1
11B	1.46	78.4 ± 15.2
A	0.37	28.6 ± 1.9

TABLE 9 Results of EPR measurements at SE on plates cut from the weld: grain size ASTM (X100) 5.5. Note also the results of three oxalic acid etch tests.

Distance from fusion line, mm	P_a C/cm²	Oxalic acid etch
0.7	2.1	
2.3	9.8	
3.2	18.7	Ditch
3.7	18.3	
4.8	15.2	
5.7	10.6	Ditch
7.3	5.1	Ditch
8.2	1.0	
9.8	0.4	
10.7	0.3	
12.3	0.3	

TABLE 10 Results of IBAS analysis of oxalic acid etch structures on the longitudinal HAZ section. Classification of structures as ditch, dual or step was performed manually.

Field no	Distance from fusion line (mm)	% ditched grain boundaries (oxalic acid etching)			
		Side 1		Side 2	
1	0.2	56		56	
2	0.6	59		51	
3	1.0	53		63	
4	1.4	58		60	
5	1.8	84		78	
6	2.2	84		77	
7	2.6	79		85	Ditch
8	3.0	80		81	
9	3.4	87		80	
10	3.8	83	Ditch	78	
11	4.2	83		77	
12	4.6	84		74	
13	5.0	85		69	
14	5.4	85		65	
15	5.8	82		45	
16	6.2	69		28	Dual
17	6.6	68		6	
18	7.0	61		-	
19	7.4	57		-	
20	7.8	36	Dual	-	Step
21	8.2	26		-	
22	8.6	7		-	
23.	9.0	2	Step		

TABLE 11 Composition of matrix, δ-ferrite near the fusion line, carbides at the phase and grain boundaries in wt.% obtained by ATEM.

	Fe	Cr	Ni	Mo	Mn	Si
Matrix, γ	68.7	19.3	9.4	-	1.3	0.9
Ferrite, δ	65.3	27.2	3.8	1.6	0.8	1.1
Particles, $M_{23}C_6$, γ/δ-boundary	29.1	64.3	2.1	3.2	1.1	-
Particles, grain boundary, $M_{23}C_6$	11	87	0.7	1.3	-	-

TABLE 12 The number and size of the grain boundary carbides in the studied TEM specimens.

Distance from the fusion line mm	Number of the carbides per μm²	Average size nm	Max. size nm
1.0	only locally	-	(200-300) x (150-200)
2.5	32	114 x 71	300 x 160
4.0	43	71 x 42	180 x 80
5.5	56	43 x 35	160 x 60
7.0	only locally	-	10 - 20
9.5	-	-	-

TABLE 13 Test schedule for SSRT of welded specimens from Ringhals 1 in water at 250 °C.

Specimen No	Electrode potential mV(SHE)	Preload N/mm²	Elongation rate mm/min
NKA 2	-250	-	5.8×10^{-4}
NKA 3	-200	-	5.8×10^{-4}
NKA 4	Air-sat.	220	7.5×10^{-5}
NKA 5	Air-sat.	150	7.5×10^{-5}

TABLE 14 Results from SSRT of welded specimens from Ringhals 1 in water at 250 °C.

Specimen No	Electrode potential mV(SHE)	Pre-exposure h	Time to failure h	Specimen contraction Z, %	$\frac{S_{scc}}{S_o}$ %	Fracture surface
NKA 2	-250	96	238	50	0	dimple
NKA 3	-200	24	266	60	0	dimple
NKA 4	Air-sat.	192	410	4	96	IGSCC
NKA 5	Air-sat.	192	331	12	88	IGSCC

TABLE 15 Environmental data during SSRT in water at 250 °C.

Specimen No.	Electrode potential mV(SHE)	Oxygen conc. µg/kg	Conductivity 25 °C Inlet µS/cm	Outlet µS/cm
NKA 2	-250	9 - 15	<.08	.10 - .12
NKA 3	-200	25 - 40	<.08	.16 - .19
NKA 4	-	Air-sat	-	-
NKA 5	-	Air-sat	-	-

TABLE 16 Multipotential test results.

Test potential	Distance from the fusion line (mm) 1.0	3.5	6.0	8.5	20.0
0	NP	NP	C	N	N
-100	NP	C	C	N	N
-150	N	N	N	N	N
-200	N	N	N	N	N
-250	N	N	N	N	N

C = cracking

N = no cracking

P = pitting

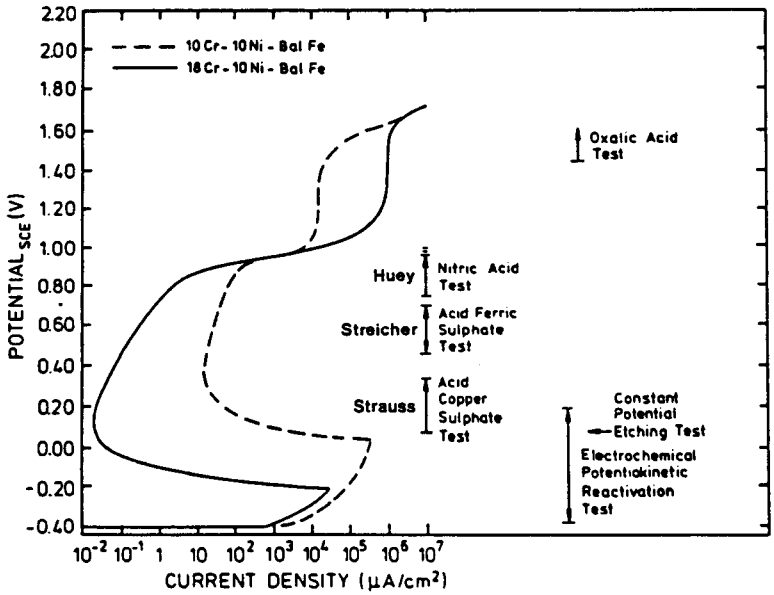


Fig. 1. Schematic illustration of the polarization behaviour of an AISI 304 type steel (18Cr10Ni) and a simulated depleted grain boundary alloy (10Cr10Ni) showing the potential regions in which standard intergranular corrosion tests are conducted (18, 21).

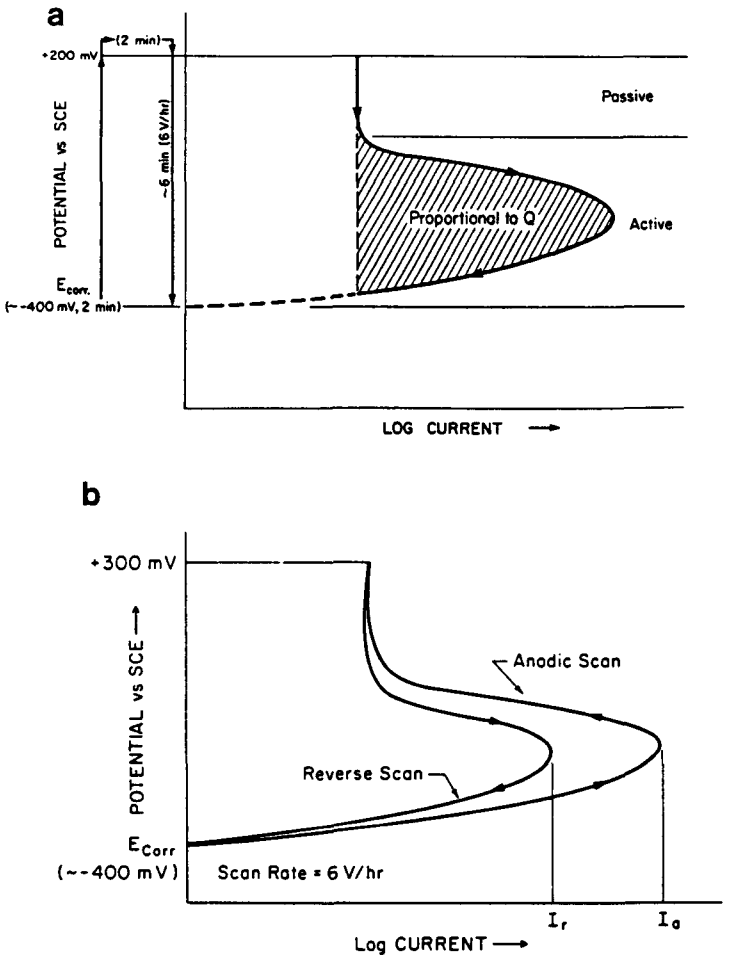


Fig. 2. Schematic illustration of the single (a) and double (b) loop EPR-techniques (16, 17).

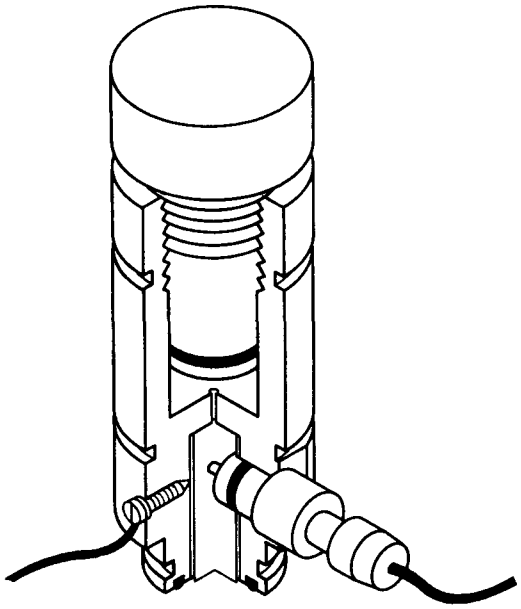
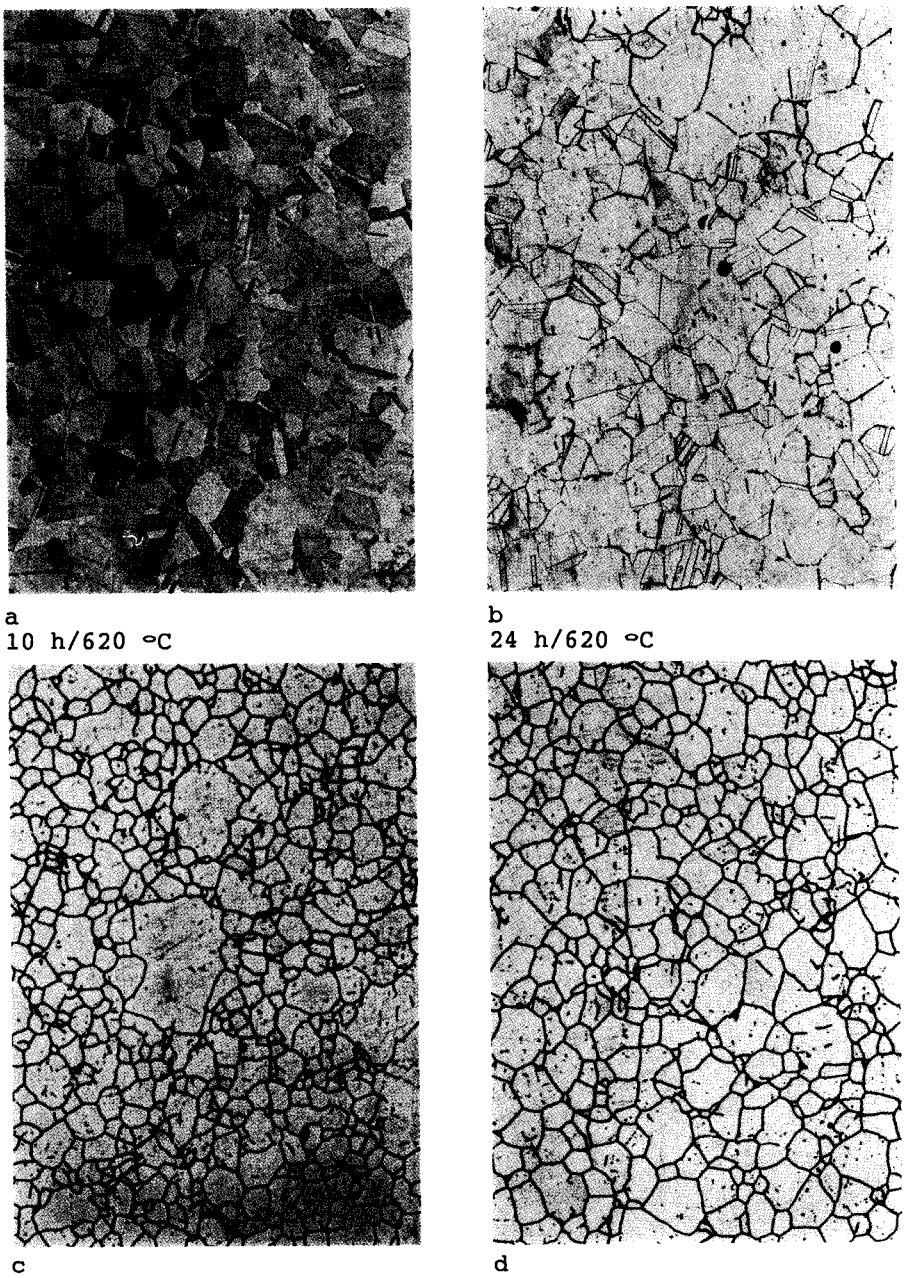


Fig. 3. Field cell used for EPR-measurements at VTT.



a
10 h/620 °C

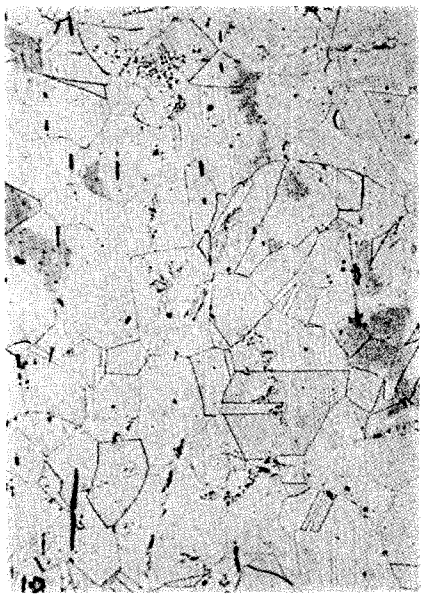
b
24 h/620 °C

c

d

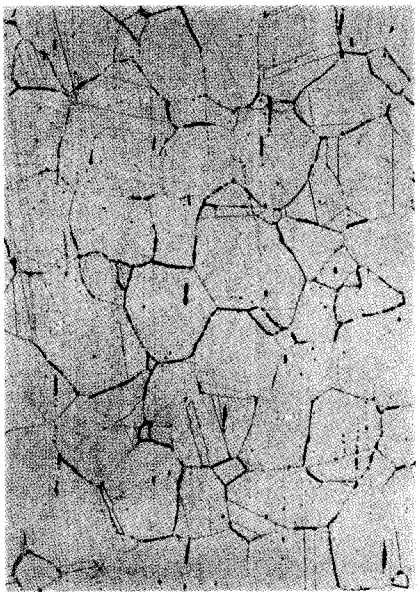
Fig. 4. Microstructures after single loop EPR testing at VTT of the round robin specimens sensitized various times at 620 °C. A field cell and test temperature of 20 °C was used. 100 x.

as-recieved



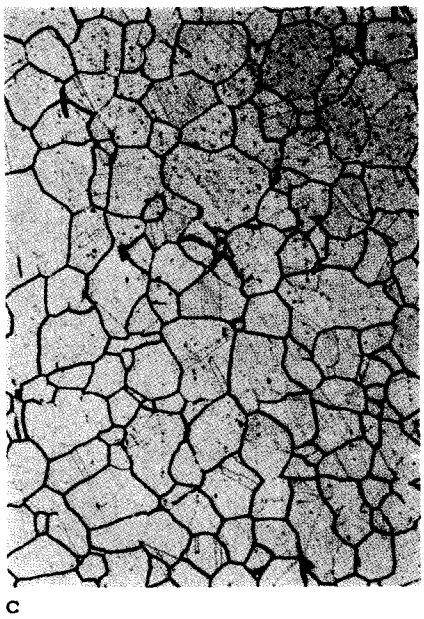
a

1 h/620 °C



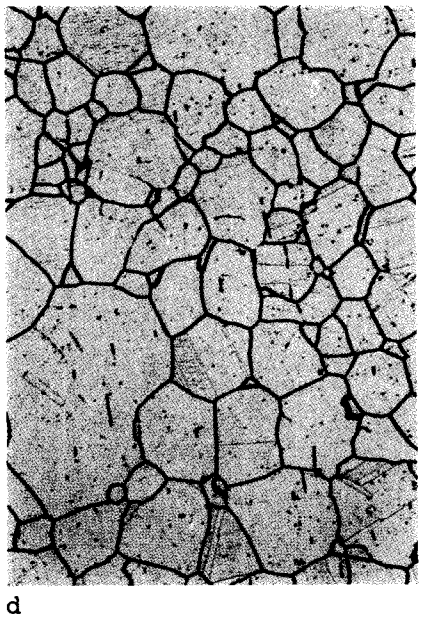
b

10 h/620 °C



c

24 h/620 °C



d

Fig. 5. Microstructures after double loop EPR testing at VTT of round robin specimens sensitized various times at 620 °C. Surface preparation before testing was polished with 1 µm diamond paste. A field cell and test temperature of 20 °C was used. 200 x.

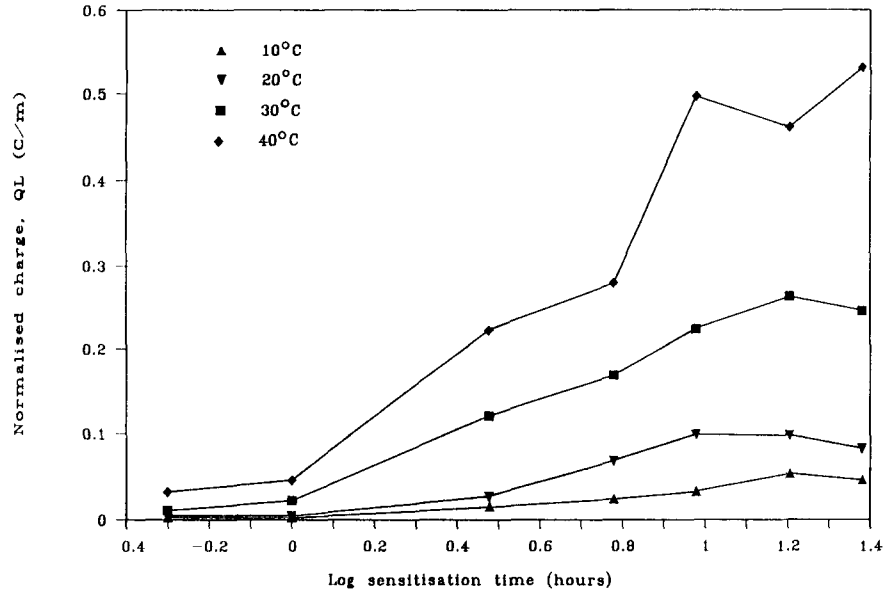


Fig. 6. Effect of sensitization time (at 620 °C) and testing temperature on the results of single loop EPR measurements.

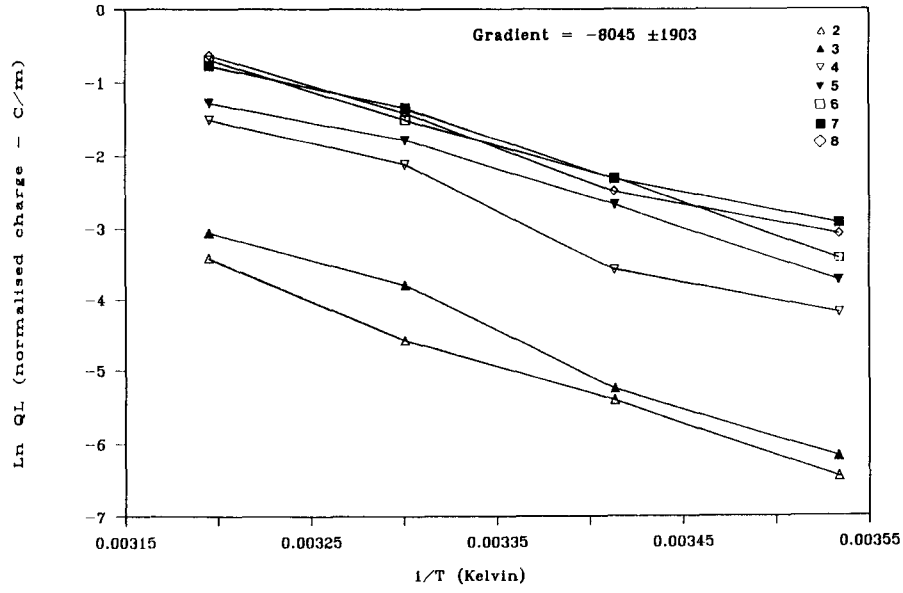


Fig. 7. Arrhenius plot of data from Table 3, giving an activation energy for dissolution of 67 ± 9 kJmol^{-1}.

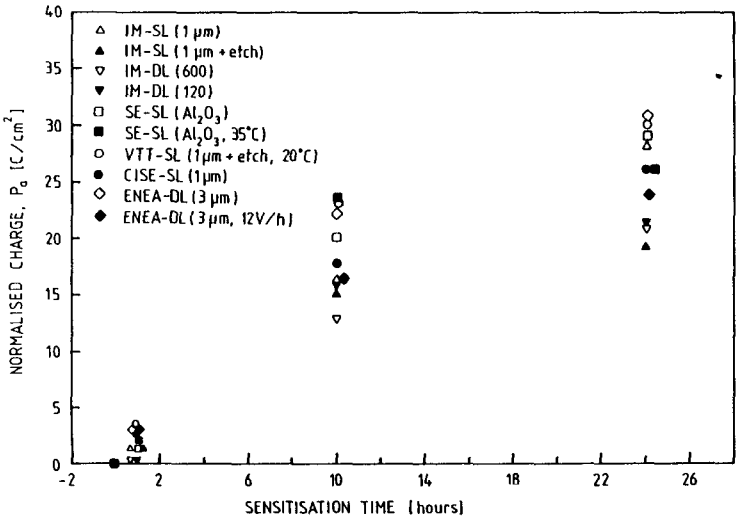


Fig. 8. Results of the European round robin EPR testing after correction for differing test temperatures and potential scan rates.

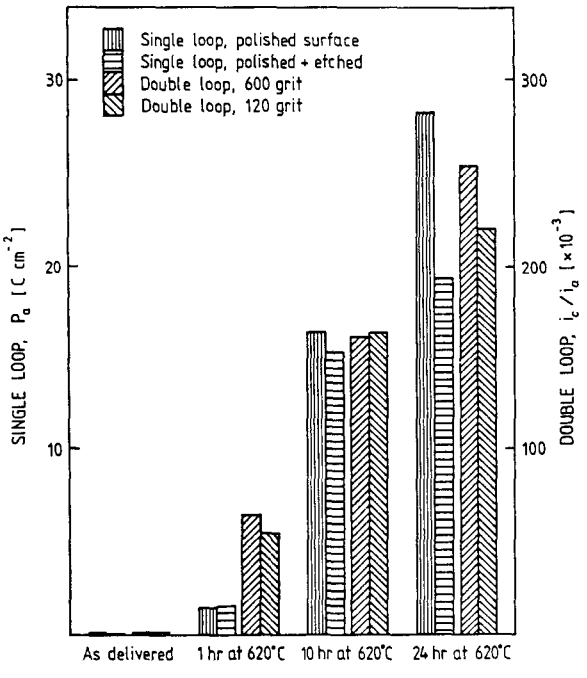
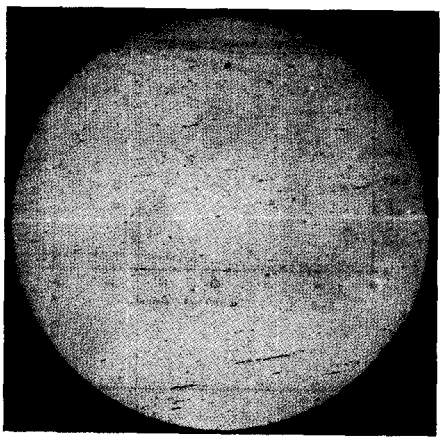


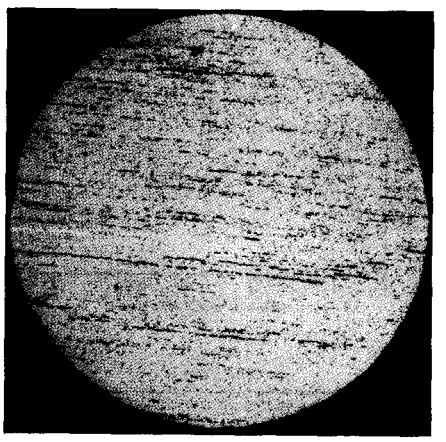
Fig. 9. Results of EPR measurements on furnace-sensitized materials after various surface treatments at IM, Sweden.

as-recieved



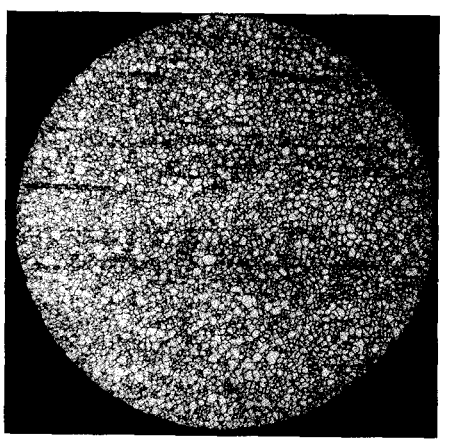
a

1 h/620 °C



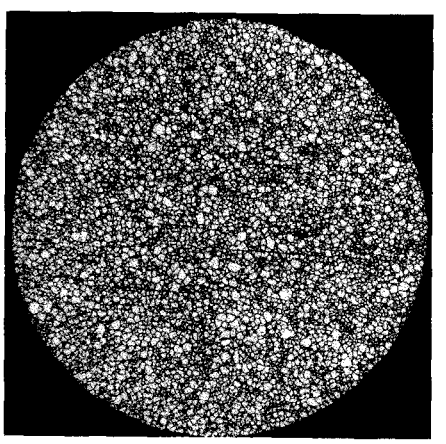
b

10 h/620 °C



c

24 h/620 °C



d

Fig. 10. Surfaces after EPR-measurements (30 °C) in the laboratory cell at VTT with furnace sensitized round robin specimens (see Table 4). 14 x.

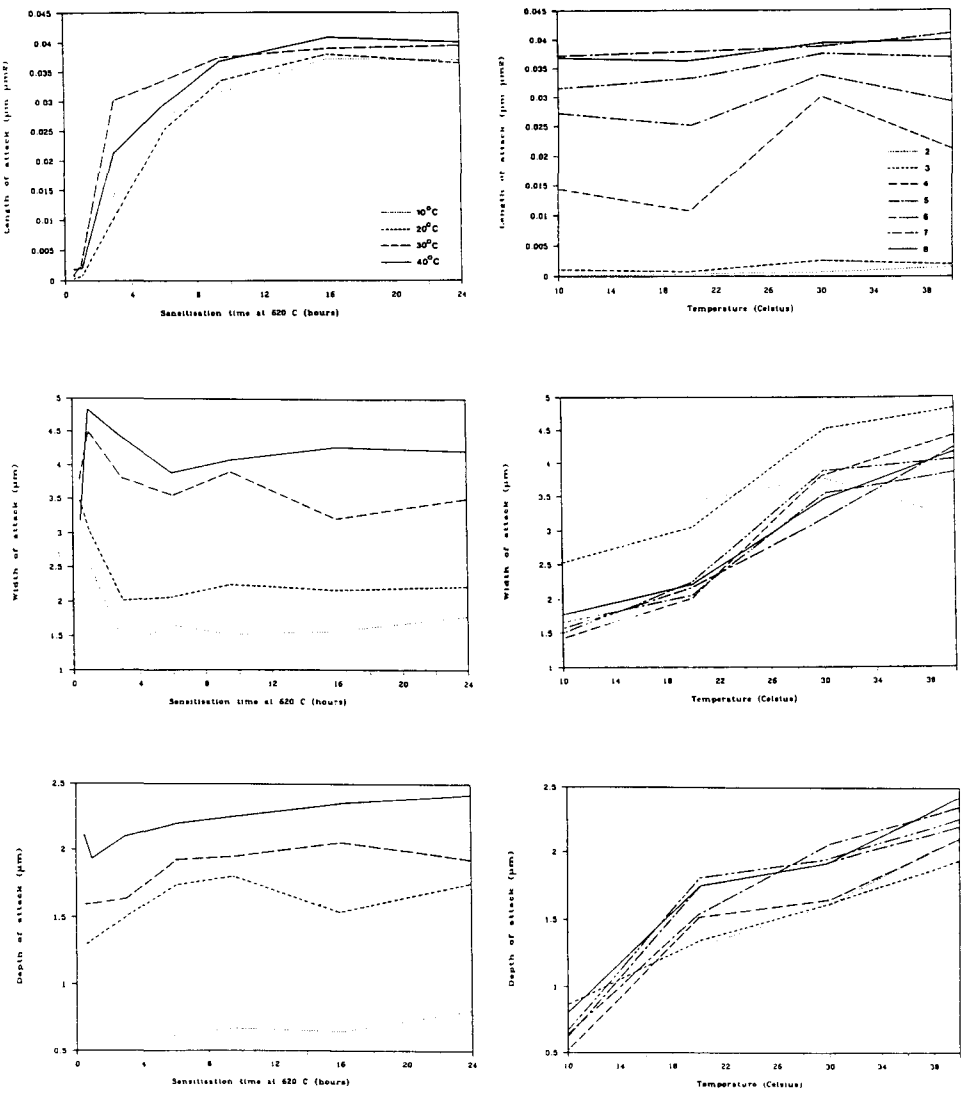


Fig. 11. Effect of sensitization time and EPR testing temperature on the length, width and depth of grain boundary attack.

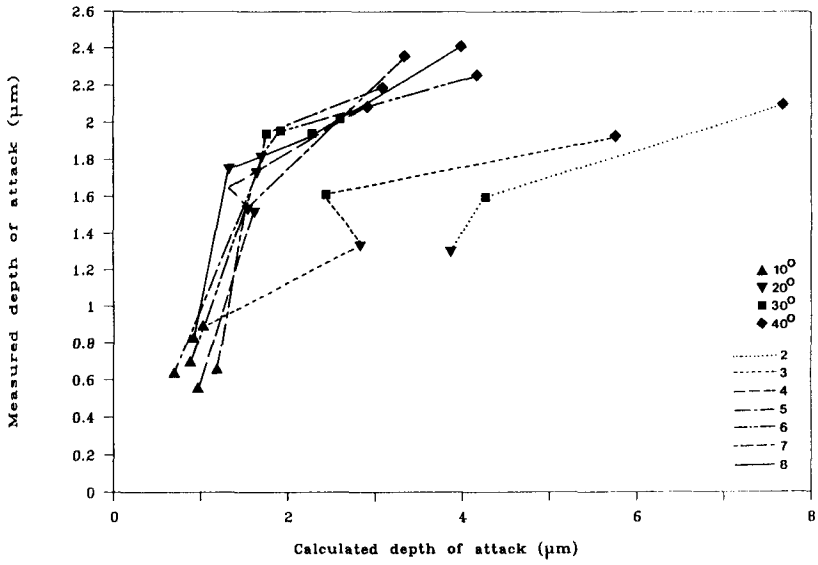
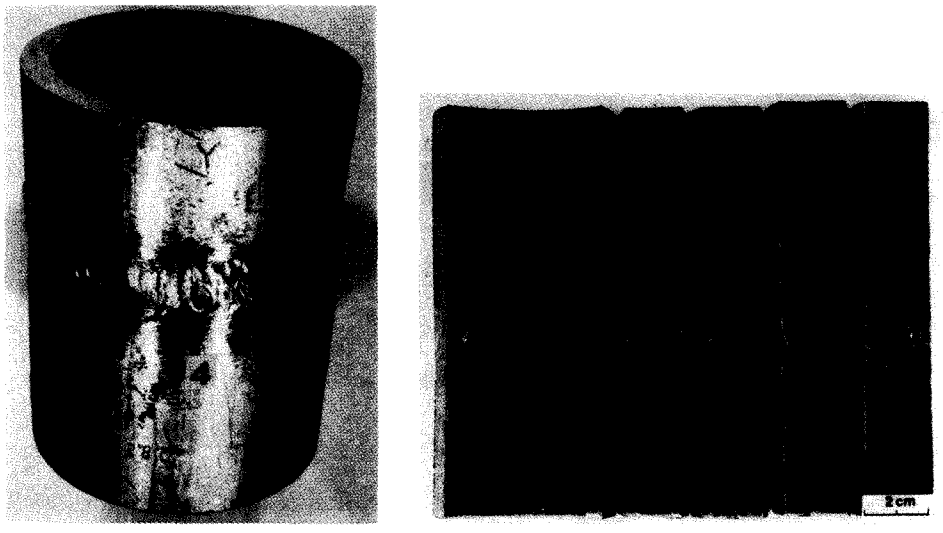


Fig. 12. Depth of grain boundary attack calculated using Equation (10) compared with the measured value at different temperatures and degrees of sensitization.



a b

Fig. 13. Pipe (114.3 x 10.0 mm) section containing a circumferential weld from Ringhals 1 BWR-plant (a) and example of sectioning the pipe for characterization of the weld heat affected zones (b).

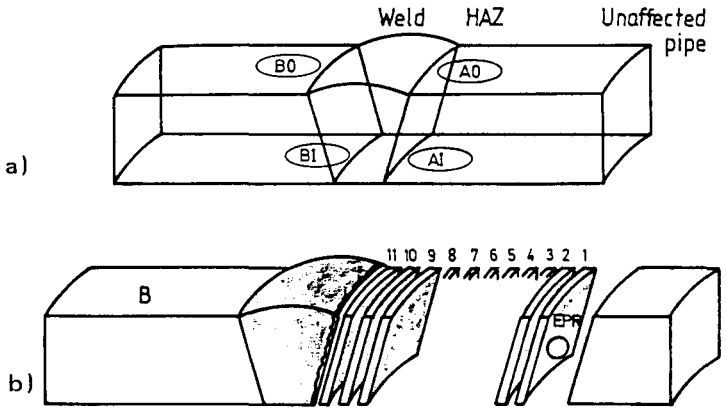


Fig. 14. (a) Areas used for EPR measurements on inner and outer pipe surfaces. (b) Sectioning of the HAZ, EPR measurements performed on both sides of each section as indicated (diameter 6 mm, tangential to inner surface of the pipe).

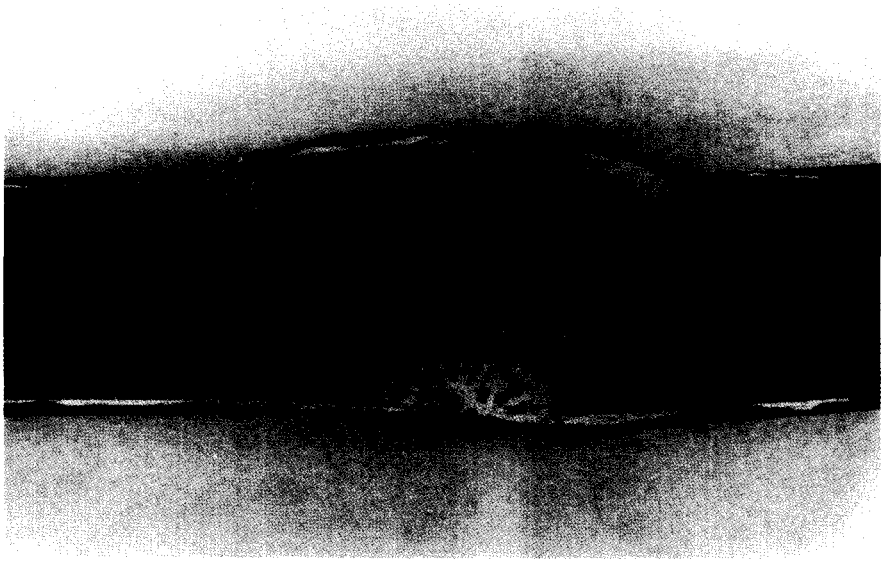


Fig. 15. Macrophotograph of the side of the welded specimen after etching in 50 ml, H_2O/50 ml HCl/5 ml HNO_3 to reveal the weld structure and sensitized areas in the HAZ.

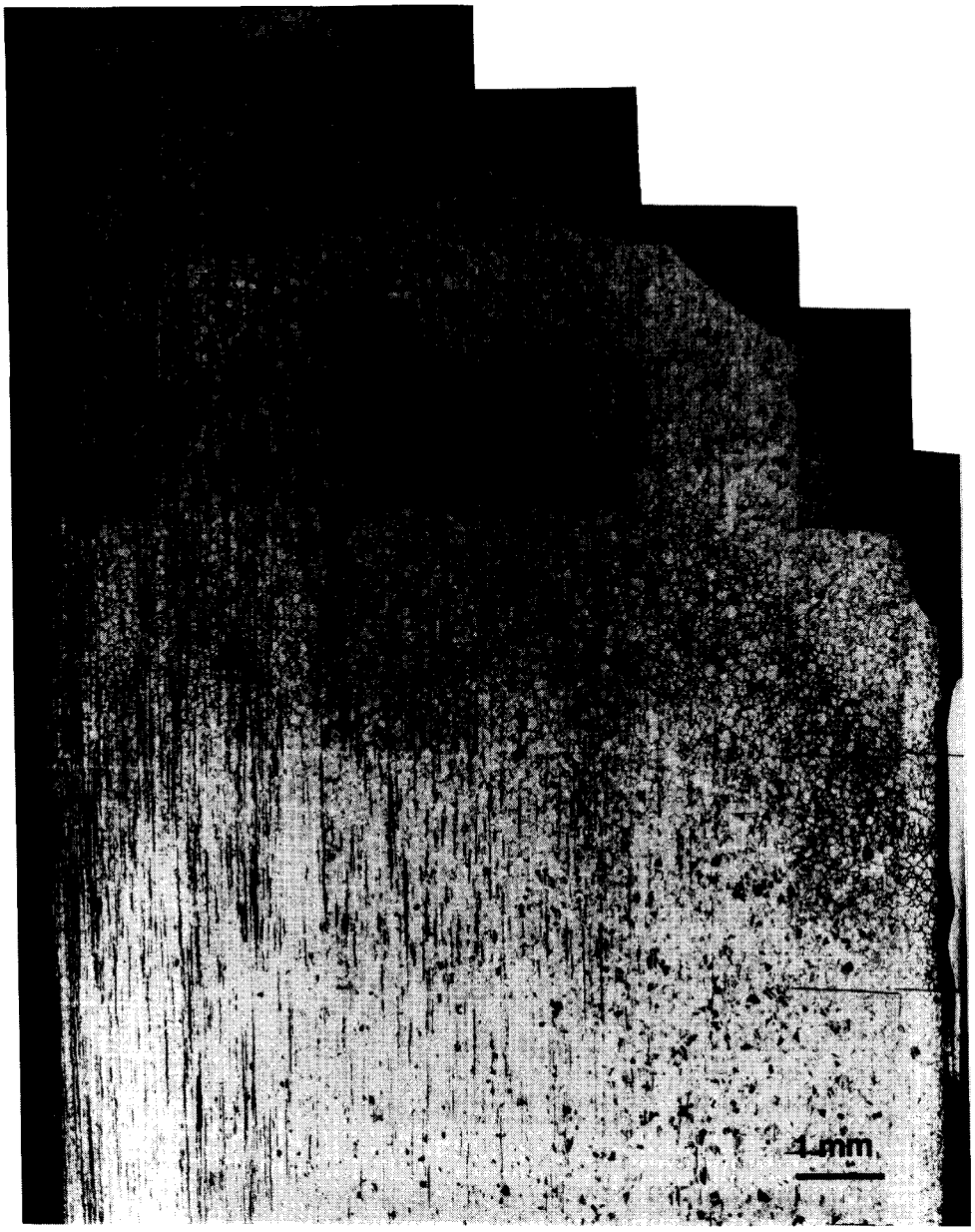


Fig. 16. More sensitized side of the HAZ etched in oxalic acid to show the form and size of the sensitization zone adjacent to the fusion line.

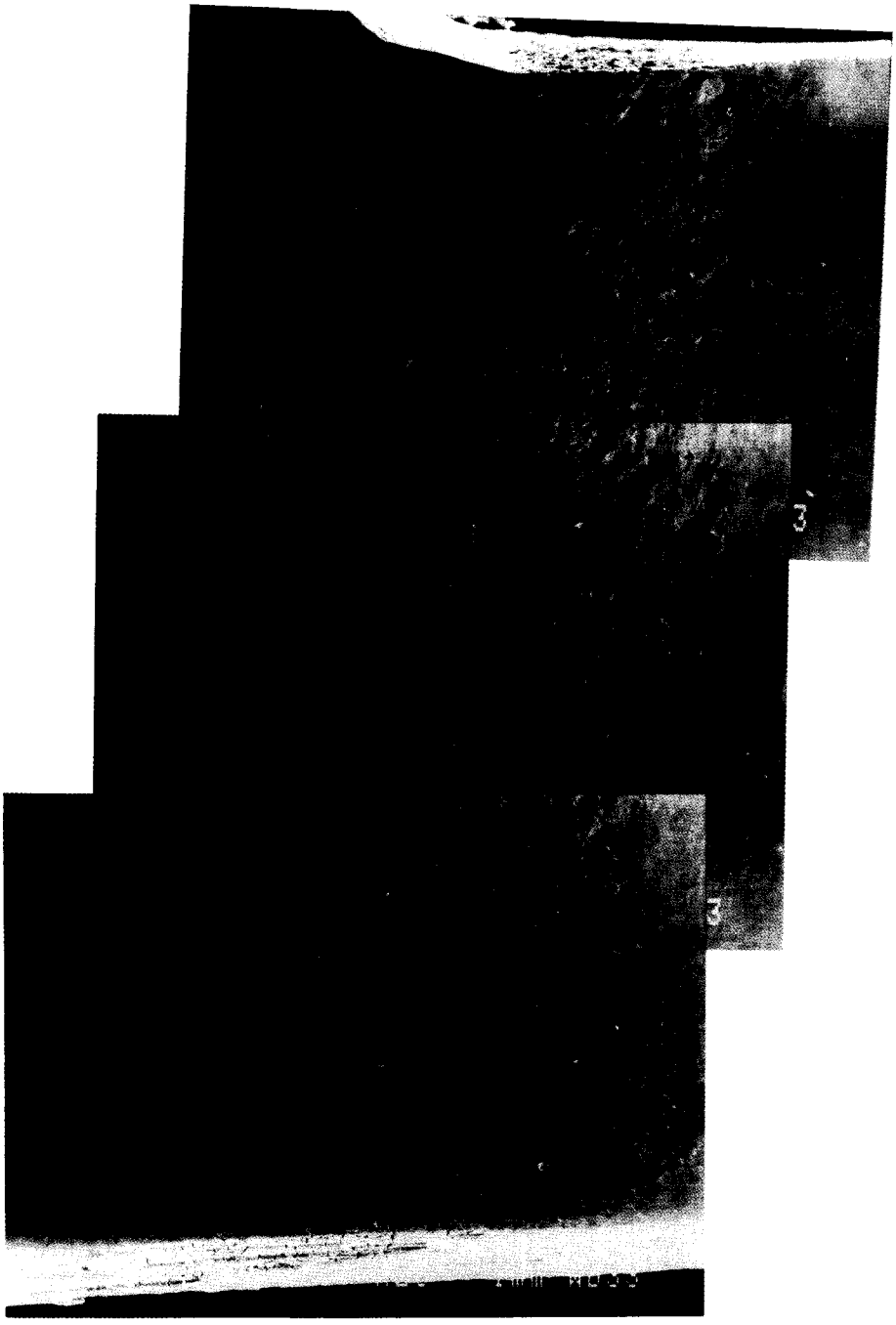
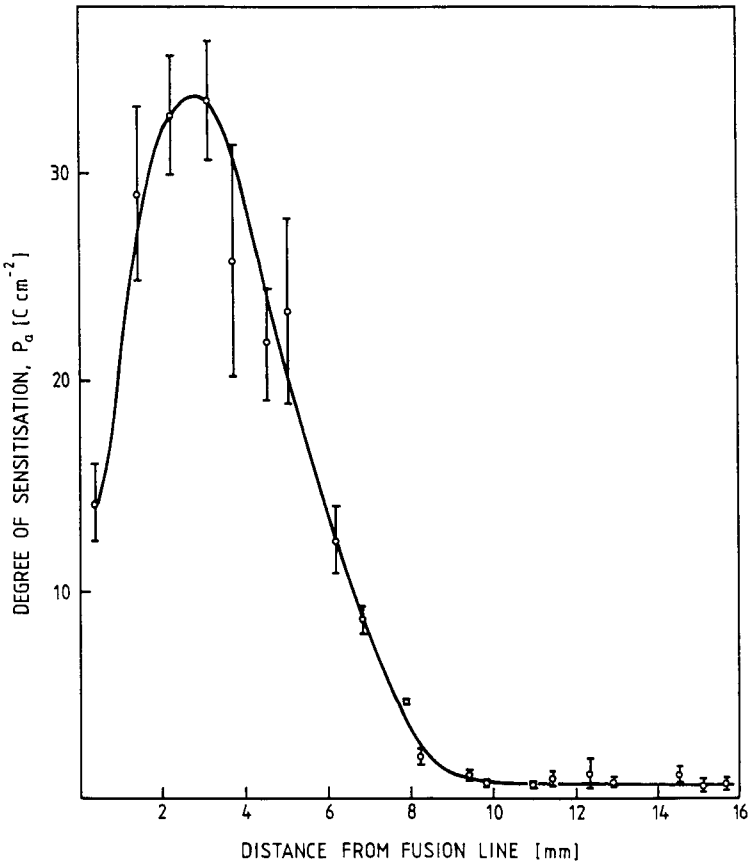
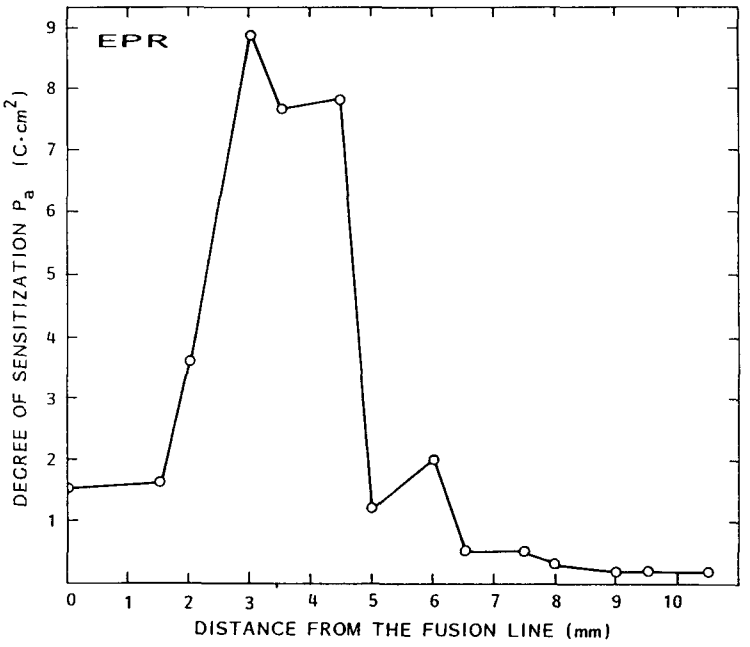


Fig. 17. Cross-section of the HAZ (weld on the left side) after Strauss test and bending of 15 degrees to reveal the attacked grain boundaries. The other side of the weld showed much narrower sensitized zone.

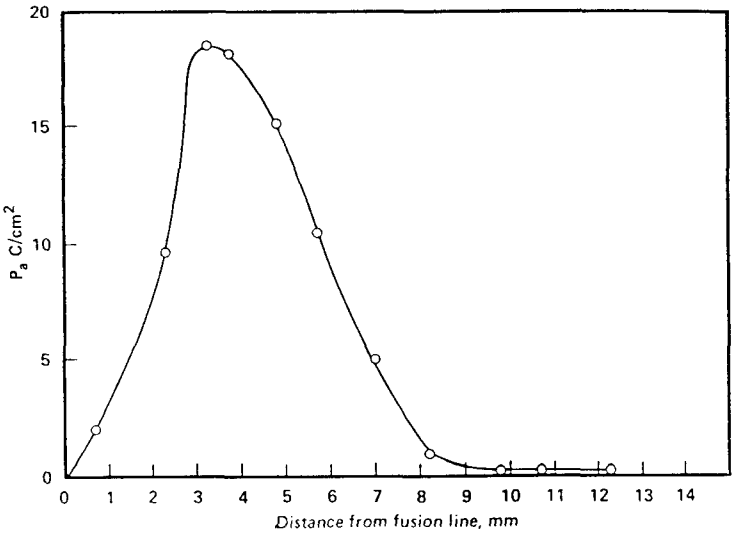


a)

Fig. 18. Results of single loop EPR measurements on the sectioned HAZ at IM (a), VTT (b) and SE (c). VTT results have been measured with the field cell at 20 °C.



b)



c)

Fig. 18. Continues.

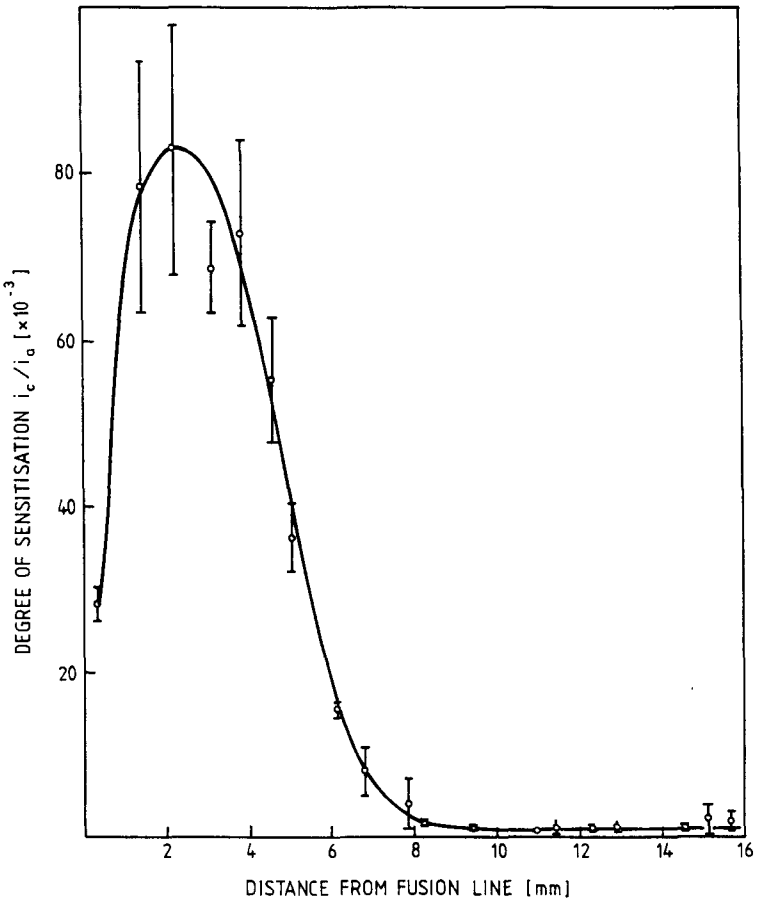
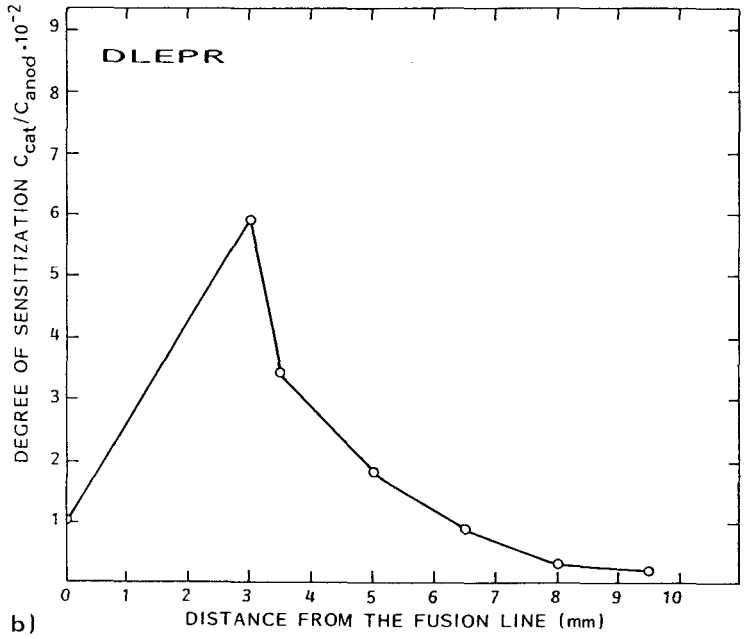
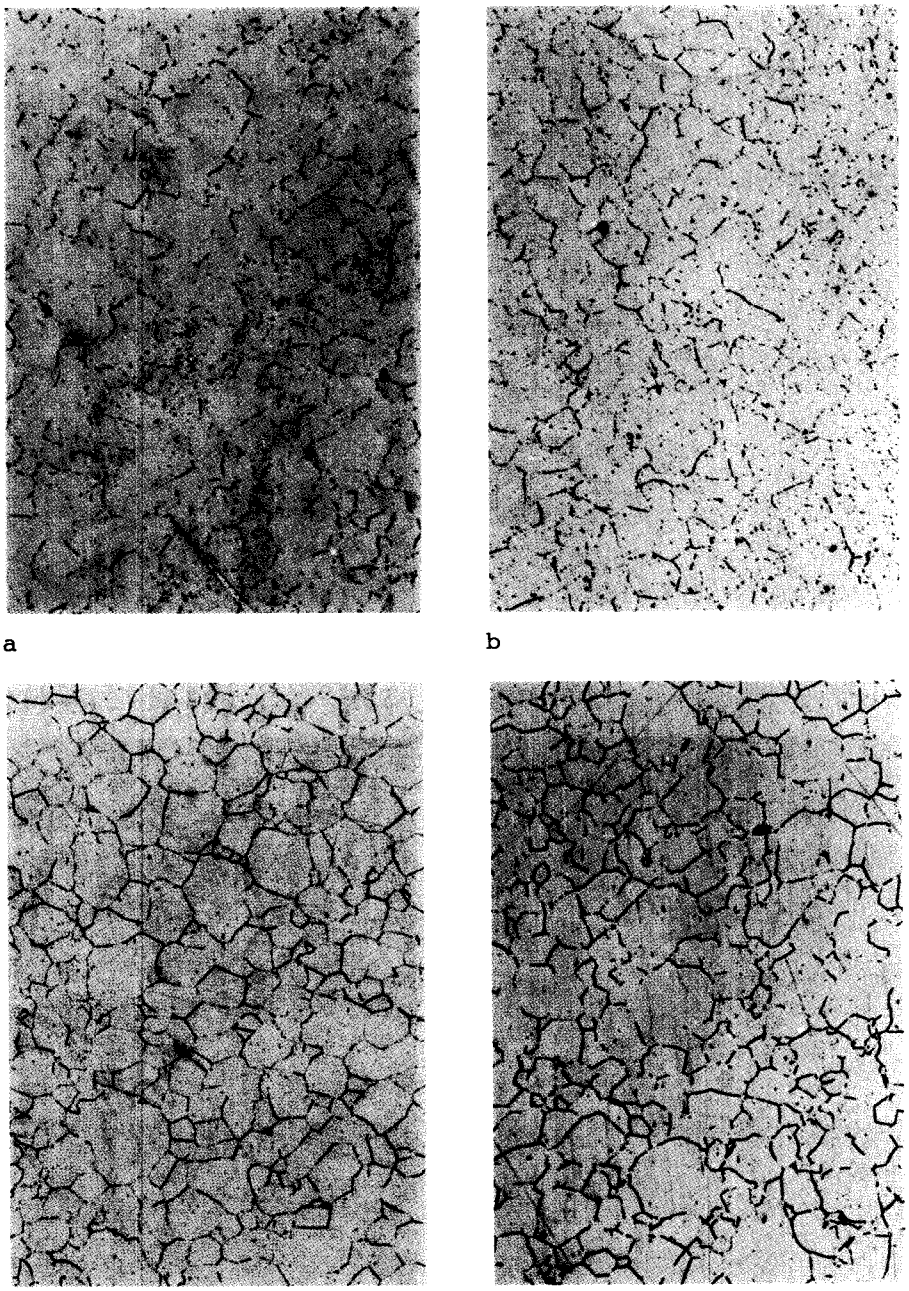


Fig. 19. Results of double loop EPR measurements on the sectioned HAZ at IM (a), and VTT (b). VTT measurements were performed with the field cell at 20 °C.



b)

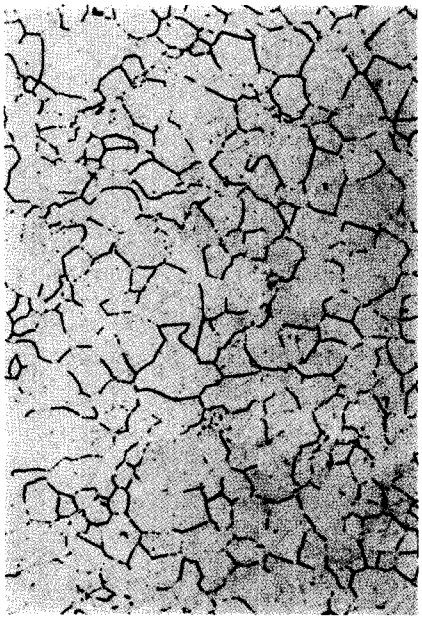
Fig. 19. Continues.



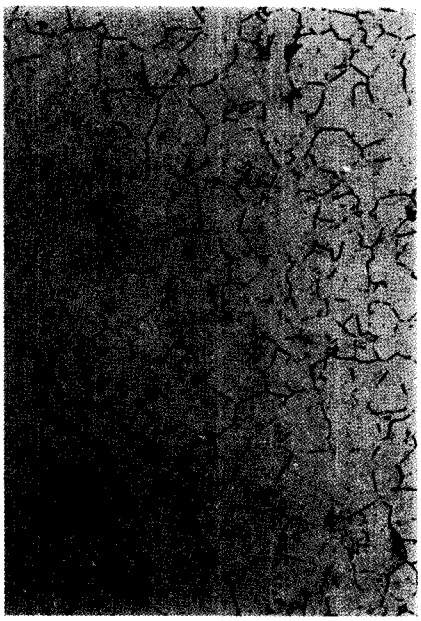
a b

c d

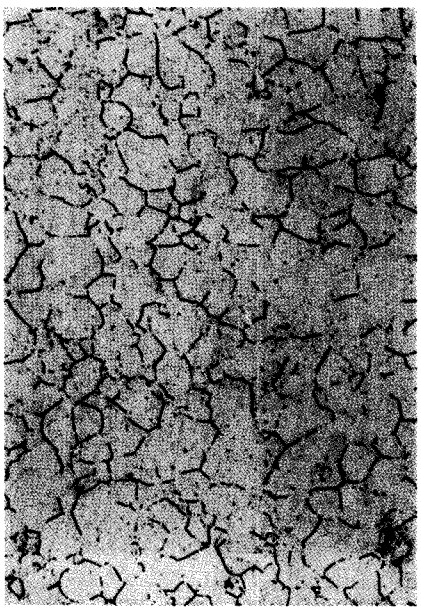
Fig. 20. Specimen surfaces after VTT single loop EPR testing from different distances from the fusion line: (a) next to fusion line, (b) 1.5 mm, (c) 2 mm, (d) 3 mm, (e) 3.5 mm, (f) 5 mm, (g) 6 mm, (h) 7.5 mm. 100 x.



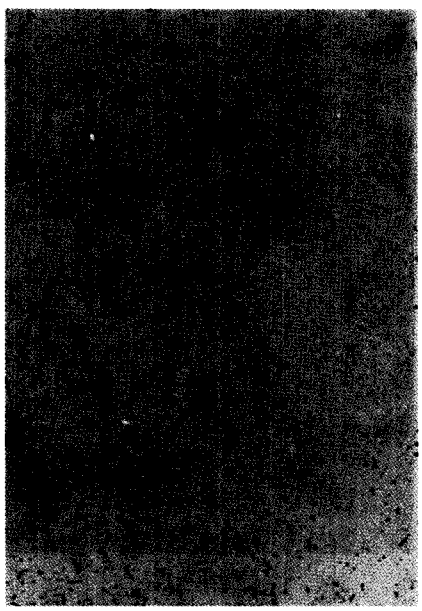
e



f



g



h

Fig. 20. Continues.

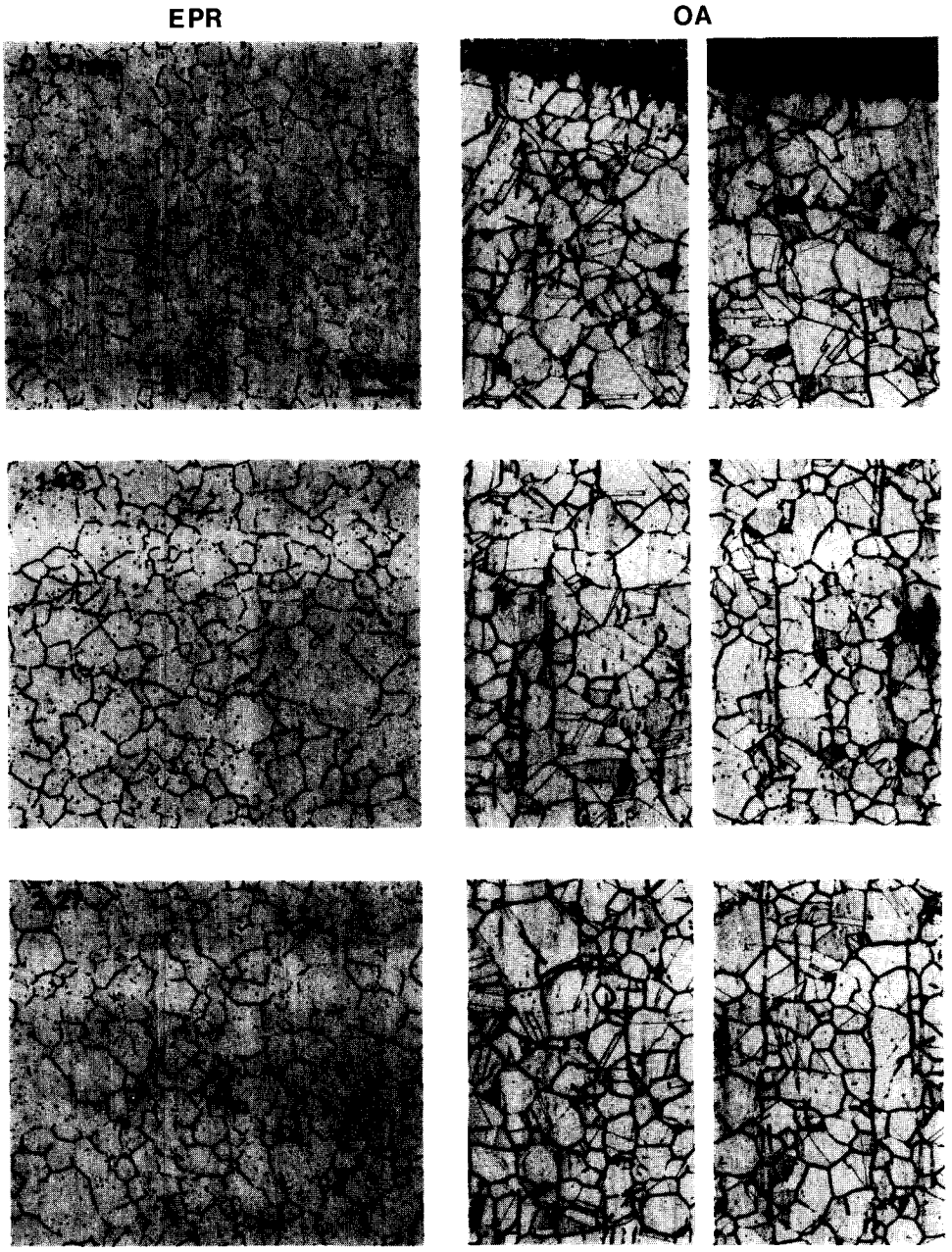


Fig. 21. Microstructures of the transversely sectioned HAZ after EPR testing at IM. Distance from the fusion line is marked on each micrograph. Also shown for comparison are the oxalic acid etch structures from the corresponding positions on the two longitudinal sections.

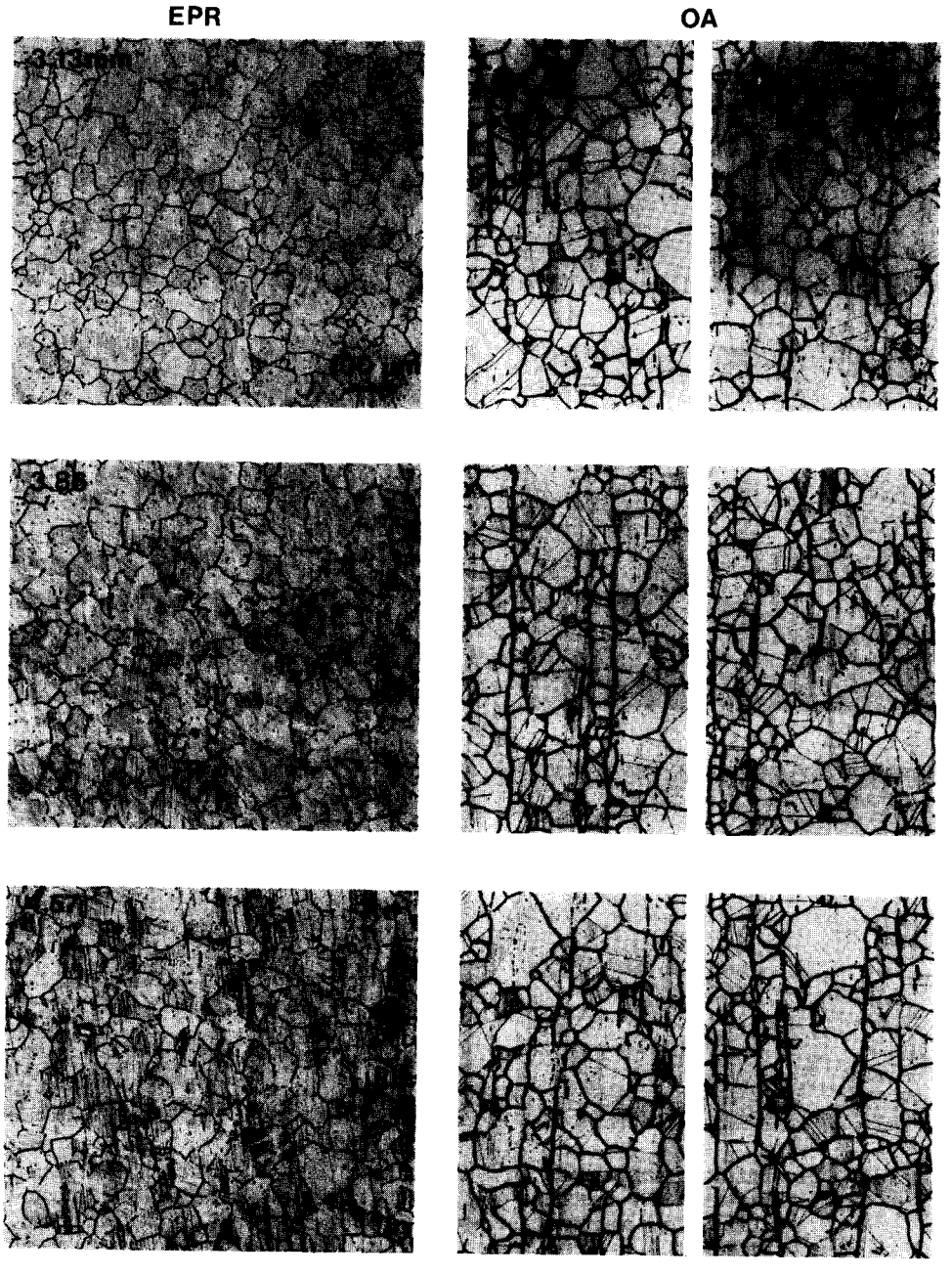


Fig. 21. Continues.

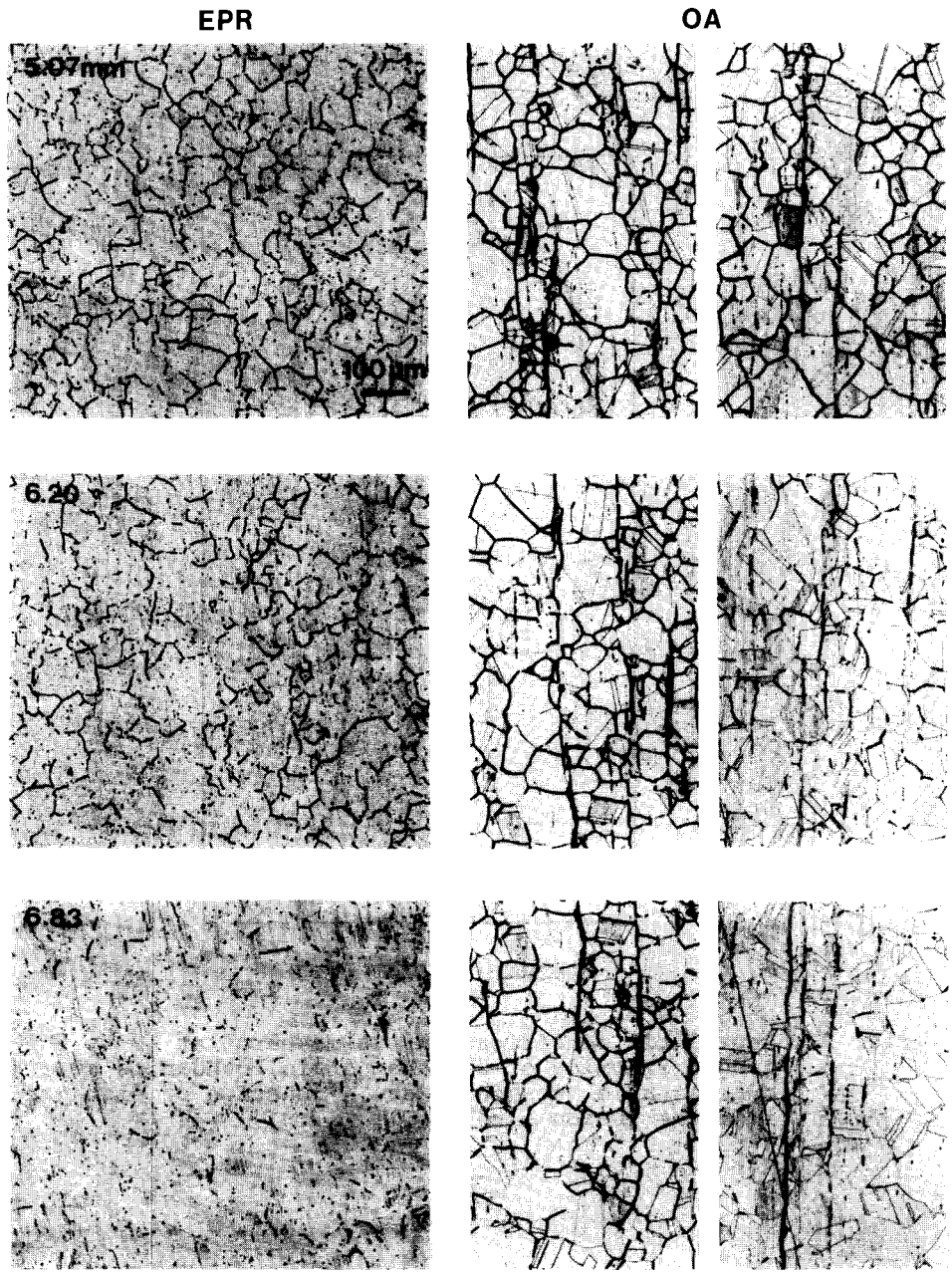


Fig. 21. Continues.

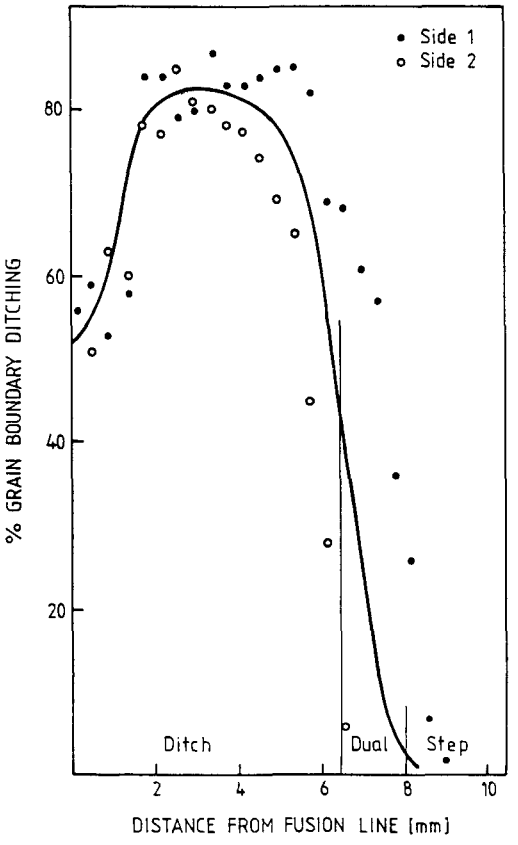


Fig. 22. Degree of sensitization, as measured at IM by the length fraction of ditched grain boundaries after oxalic acid etching, as a function of distance from the fusion line.

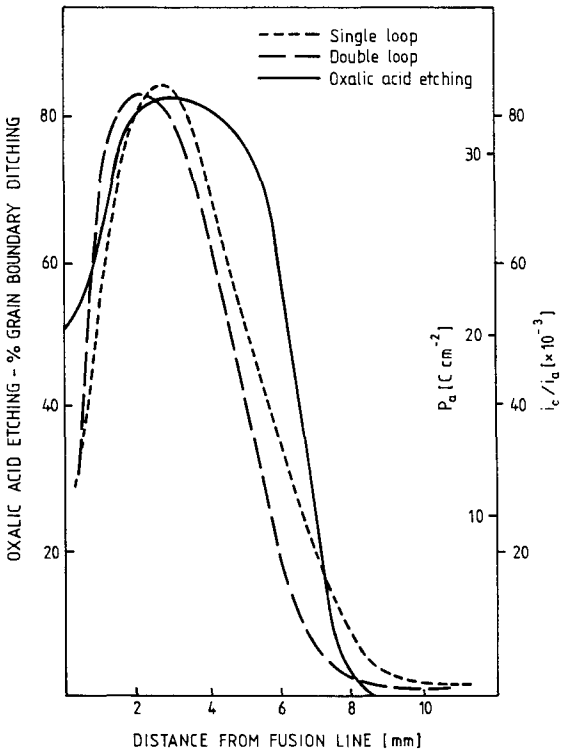


Fig. 23. Comparison between single loop, double loop and oxalic acid etch results of IM as a function of distance from the fusion line.

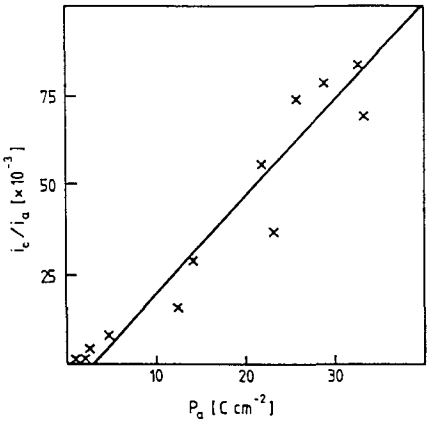


Fig. 24. Correlation between single loop measurement (P_a) and double loop (i_c/i_a) measurements of IM on the sectioned HAZ. Correlation coefficient r = 0.96.

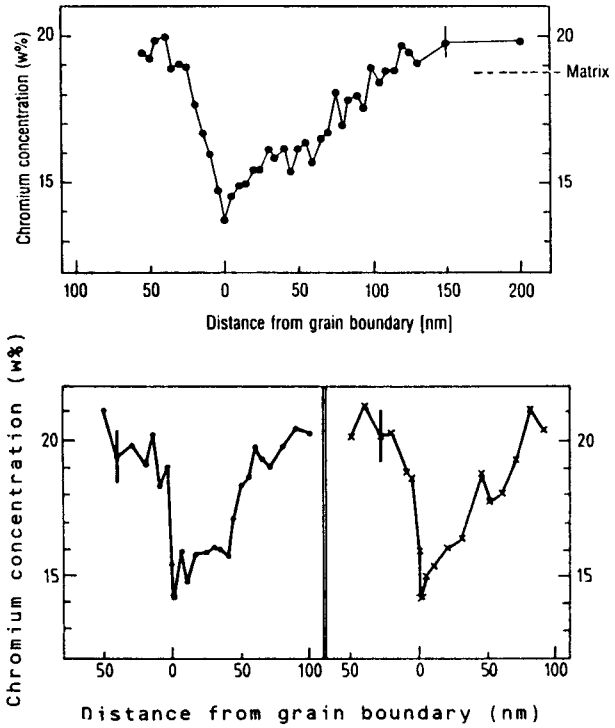


Fig. 25. Cr-depletion at the grain boundary about 1.9 mm (a) and about 3.5 mm (b) from the fusion line in the Ringhals 1 weld.

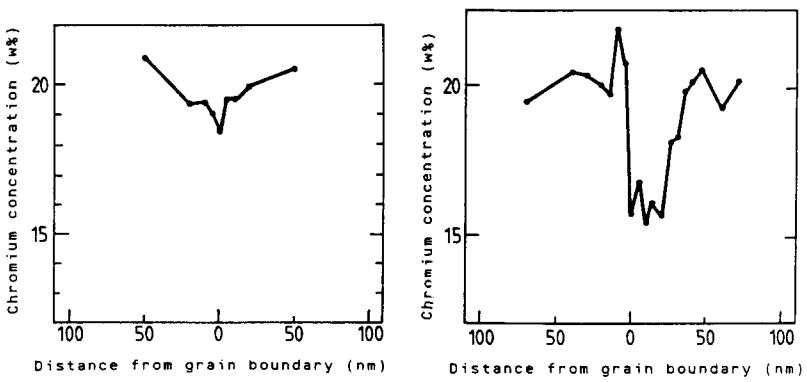


Fig. 26. Cr-depletion at the grain boundary about 4.9 mm from the fusion line in the Ringhals 1 weld (a) and about 2 mm from the fusion line in the reference weld (b) which did not have any reactor exposure.

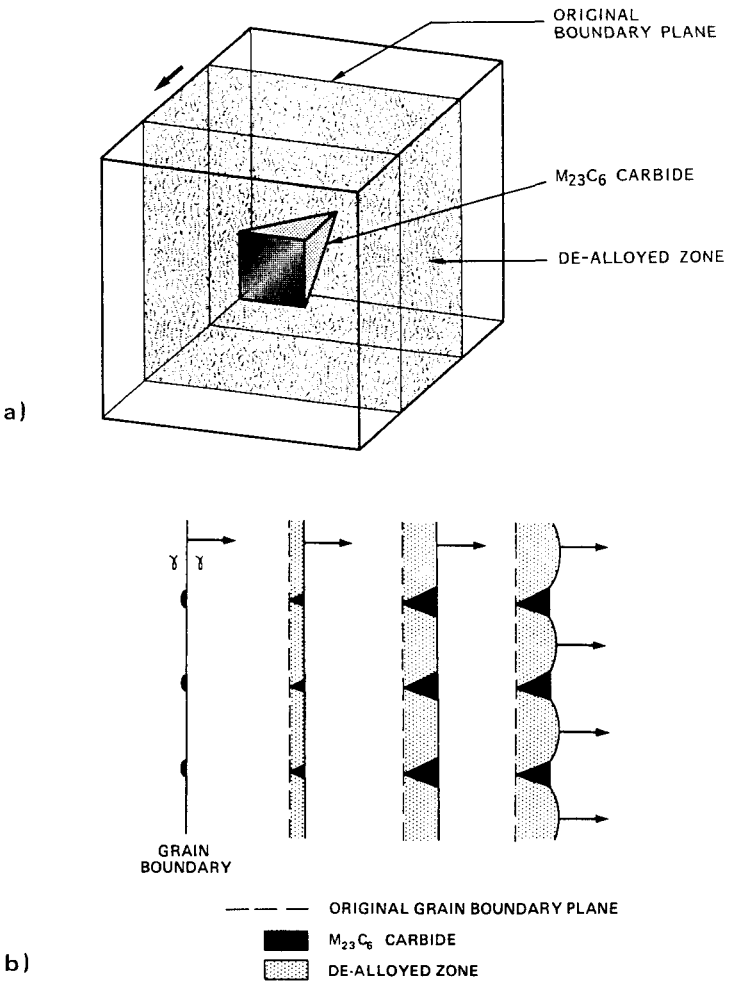


Fig. 27. (a) A schematic presentation of the growth of a $M_{23}C_6$ carbide inducing grain boundary migration. (b) A schematic presentation of the various stages of $M_{23}C_6$ carbide growth during grain boundary migration (25).

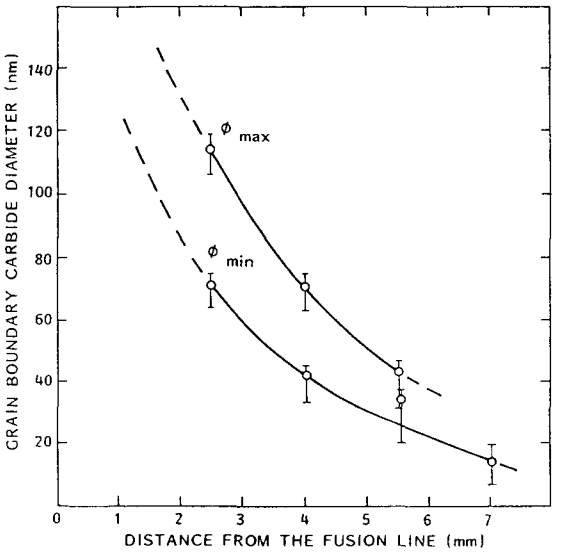
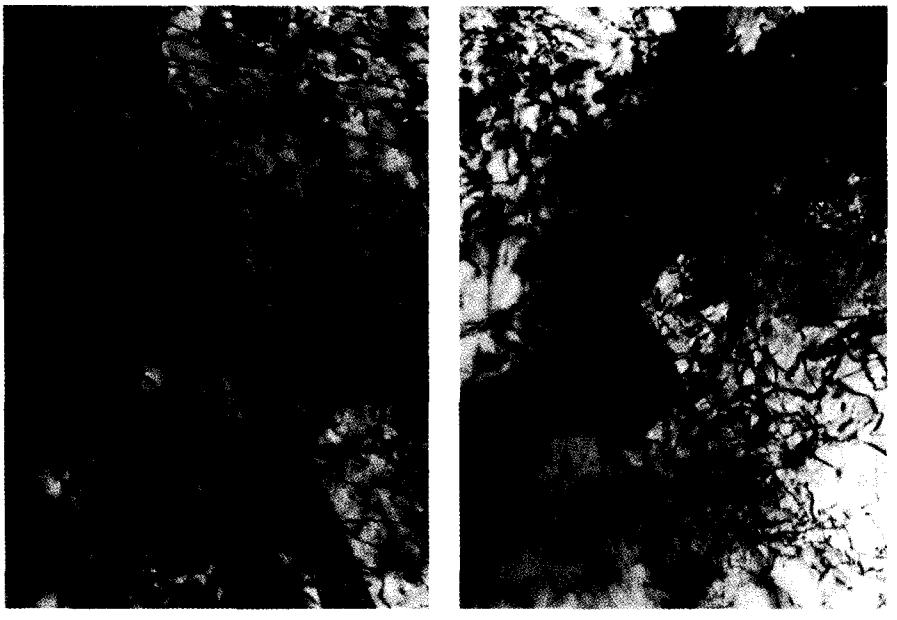
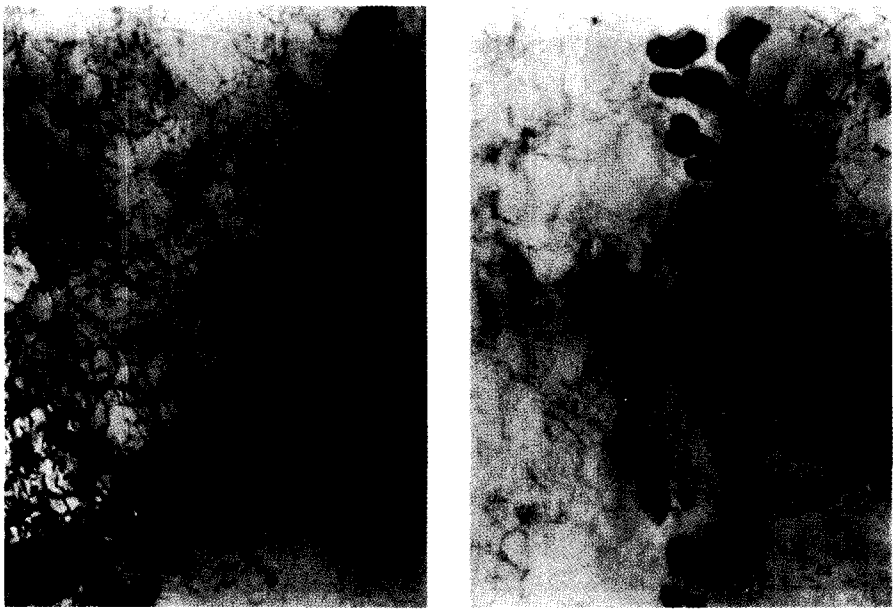


Fig. 28. The size of the grain boundary carbides as a function of the distance from the fusion line.



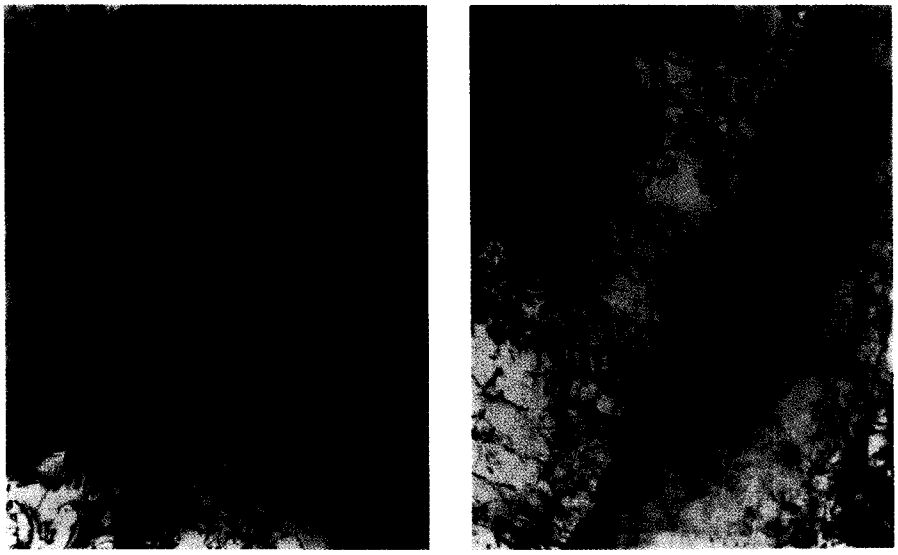
a b

Fig. 29. Grain boundaries at the distance of 1 mm from the fusion line exhibit either clean structures or occasional large carbide particles; major diameter 200 - 300 nm. 50 000x.



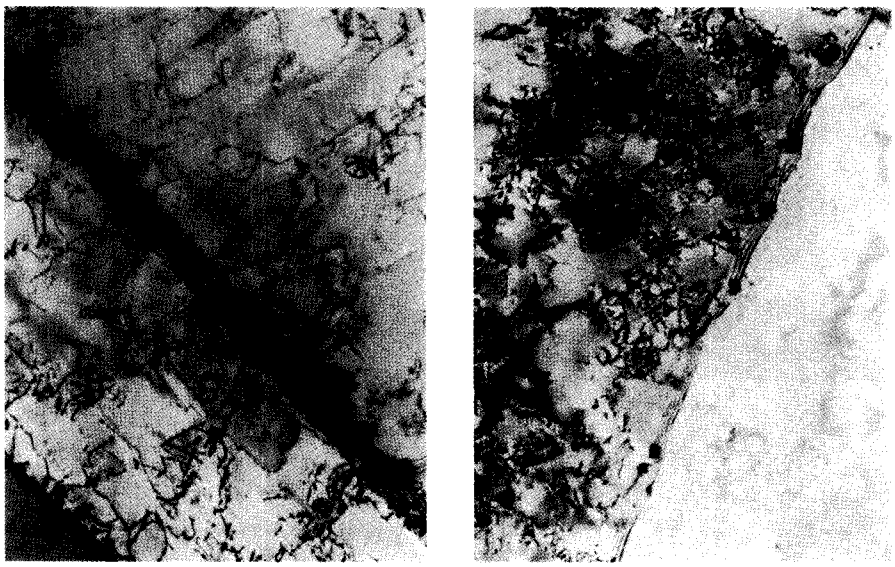
a b

Fig. 30. Grain boundaries at the distance of 2.5 mm from the fusion line exhibit large $M_{23}C_6$ carbides having a pyramide-like form. 50 000x.



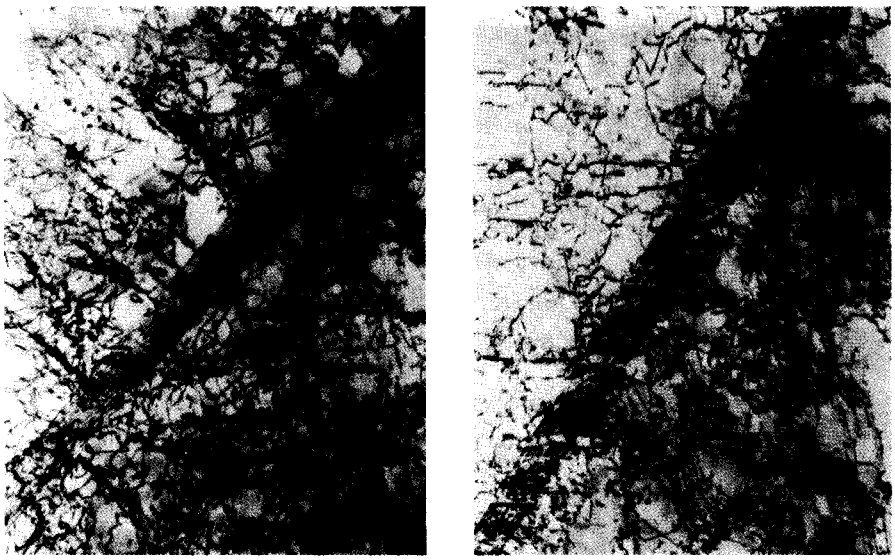
a b

Fig. 31. Grain boundaries at the distance of 4 mm from the fusion line exhibit even distribution of small carbides. 35 000x.



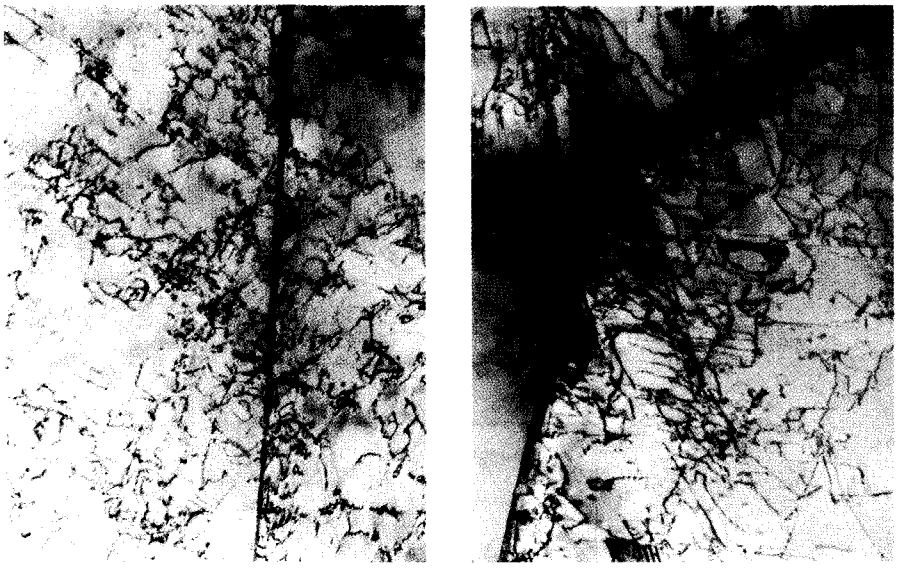
a b

Fig. 32. Grain boundaries at the distance of 5.5 mm from the fusion line exhibit an uneven distribution of small carbides. 35 000x.



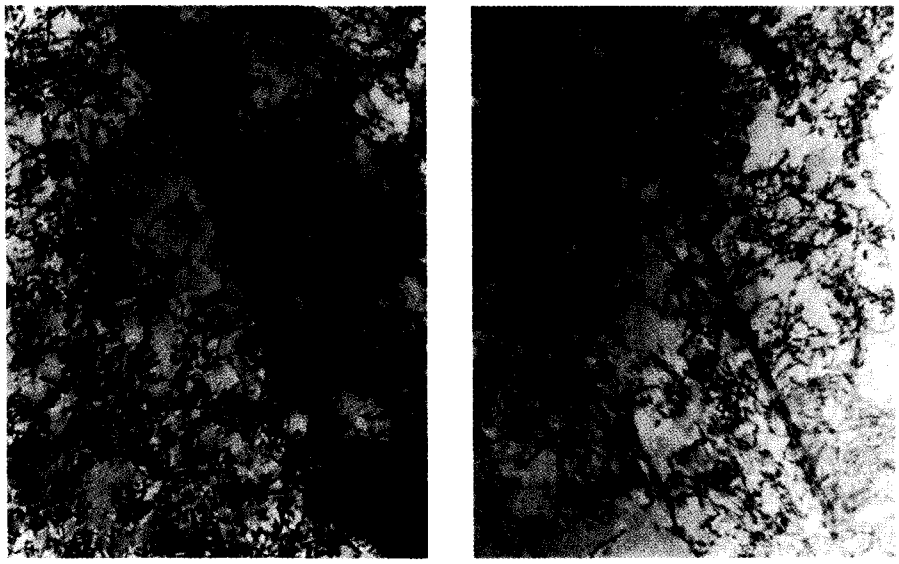
a b

Fig. 33. Grain boundaries at the distance of 7 mm from the fusion line exhibit very small carbide particles (diameter 10 - 20 nm). 35 000x.



a b

Fig. 34. Grain boundaries at the distance of 9.5 mm from the fusion line are mainly clean. Note also the slightly lower dislocation density here. 35 000x.



a b

Fig. 35. Grain boundary structures in the reference weld (without any reactor exposure) at the distances of 0.7 mm (a) and 2.7 mm (b) from the fusion line. 35 000 x

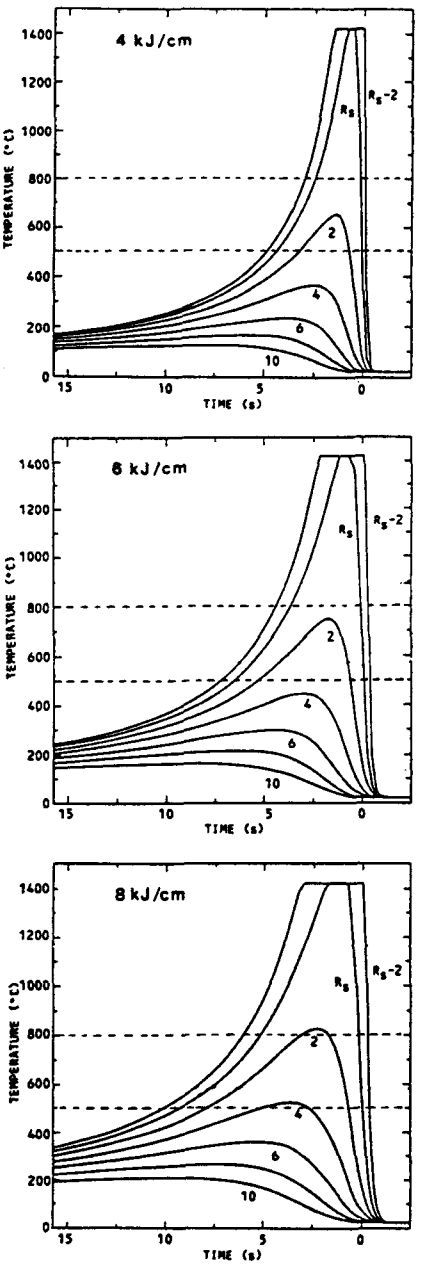


Fig. 36. Calculated temperature distribution in the HAZ for AISI 304 steel welded with different heat inputs (19). Figures indicate distance from the fusion line (R_s) in mm. Also shown is the temperature range 500 - 800 °C in which carbide precipitation predominantly occurs.

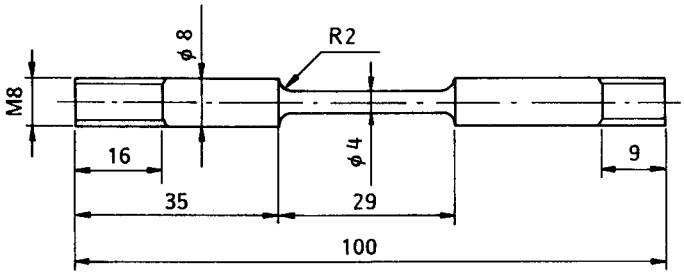


Fig. 37. Tensile specimen with dimensions in mm.

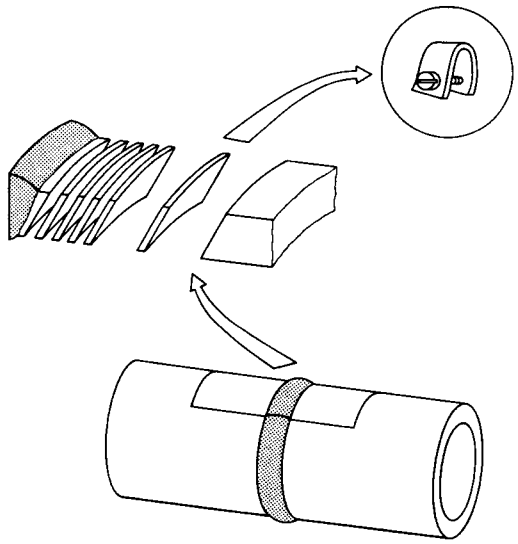


Fig. 38. Manufacturing specimens for multipotential testing.

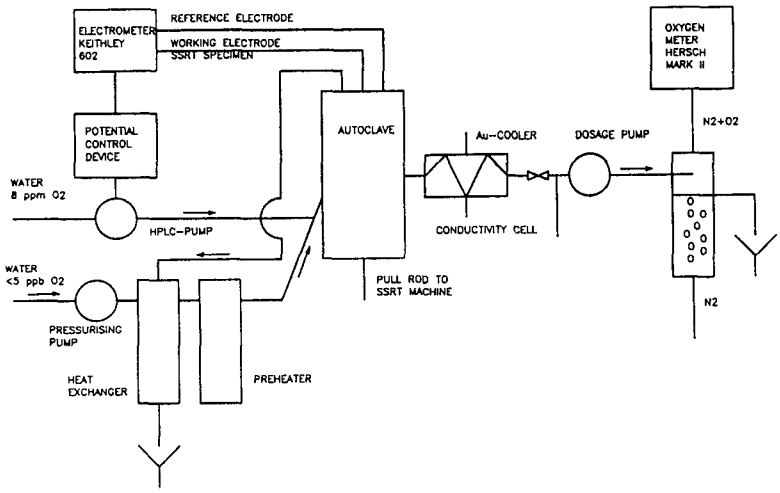


Fig. 39. Test set-up for SSRT at controlled electrode potential (6).

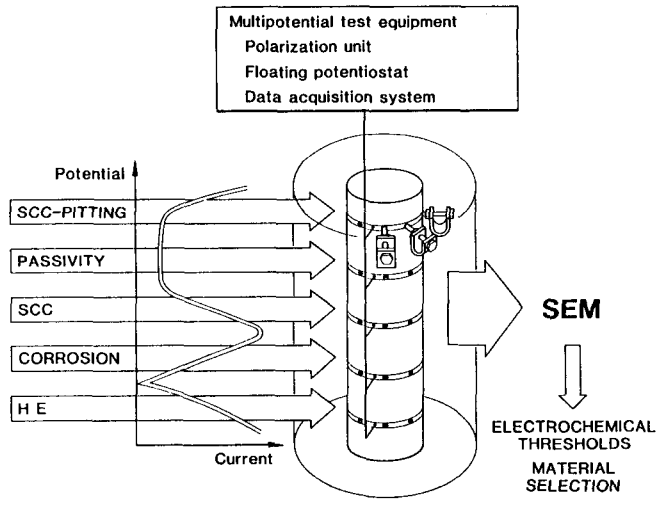


Fig. 40. Multipotential test rig.

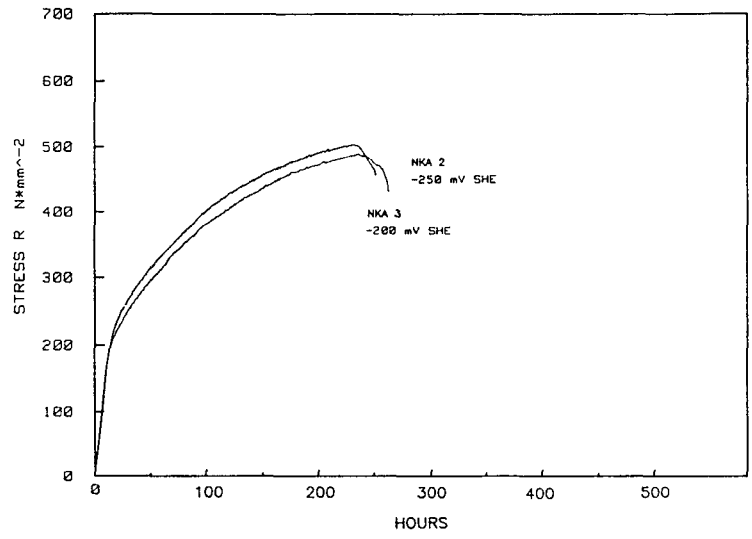


Fig. 41. Stress-time curves of SSRT-tests of welded specimens at controlled potentials in water at 250 °C.

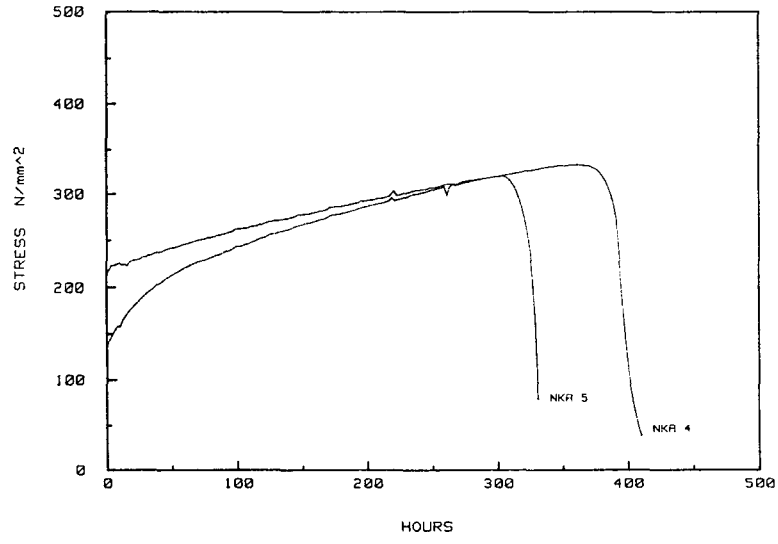
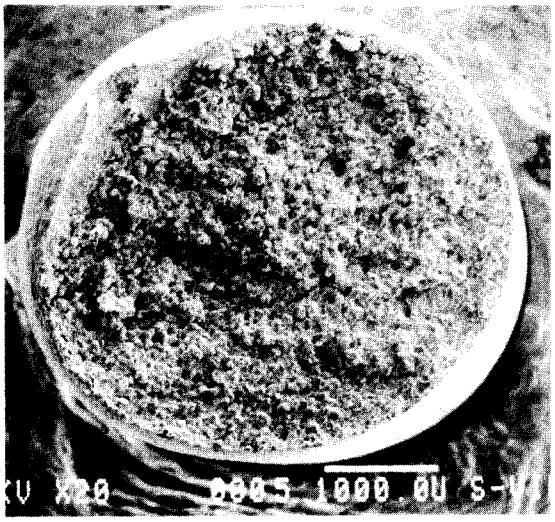
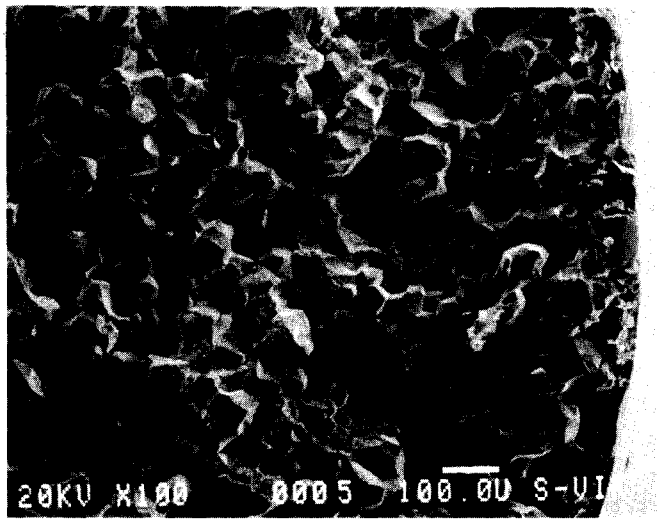


Fig. 42. Stress-time curves of SSRT-tests of welded specimens in air-saturated water at 250 °C.



X 20



X 100

Fig. 43. Specimen NKA 5 tested in air-saturated water at 250 °C. Time to failure 331 h, and S_{IGSCC}/S_o = 88 %.

LIST OF PARTICIPANTS IN THE MAT 530 -PROJECT

Finland

Technical Research Centre of Finland (VTT)	Hannu Hänninen[1] Pertti Aaltonen[2] Pertti Nenonen Kari Saarinen

Sweden

Institute for Metals Research	Rachel Jargelius Börje Lehtinen Staffan Hertzman E. Symniotis-Barrdahl
Swedish Nuclear Power Inspectorate	Margareta Trolle
Swedish Power Board	Christer Jansson[3]
Studsvik AB	Tomas Berglund Leo Germays Anders Molander Bo Rosborg Britt-Marie Svensson

[1]Project leader
[2]Project leader in 1987
[3]Material supply